Heavy Ion Collisions

A. Marin (GSI)

Spanish High Energy Physics School
Taller Altas Energías Complutense 2012

Table of Contents

Bibliography

- Ultrarelativistic Heavy-Ion Collisions. Ramona Vogt.
- Introduction to High-Energy Heavy-Ion Collisions, C.Y. Wong, World Scientific, 1994
- The physics of the quark-gluon plasma, S. Sarkar, H. Satz and B. Sinha, Lecture notes in physics, Volume 785, 2010
- Quark-Gluon Plasma Physics: from fixed target to LHC (SS2011). Prof. Dr. J. Stachel, PD Dr. K. Reygers.

  http://www.physi.uni-heidelberg.de/~reygers/lectures/2011/qgp/qgp_lecture_ss2011.html

Goals of High Energy Heavy-Ion Collisions

- Understand 2 basic properties of the strong interaction: (de)confinement, chiral symm. breaking/restoration
- Probe conditions quark-hadron phase transition in primordial Universe (few μsec after the Big Bang)
- Study the phase diagram of QCD matter: produce and study the QGP

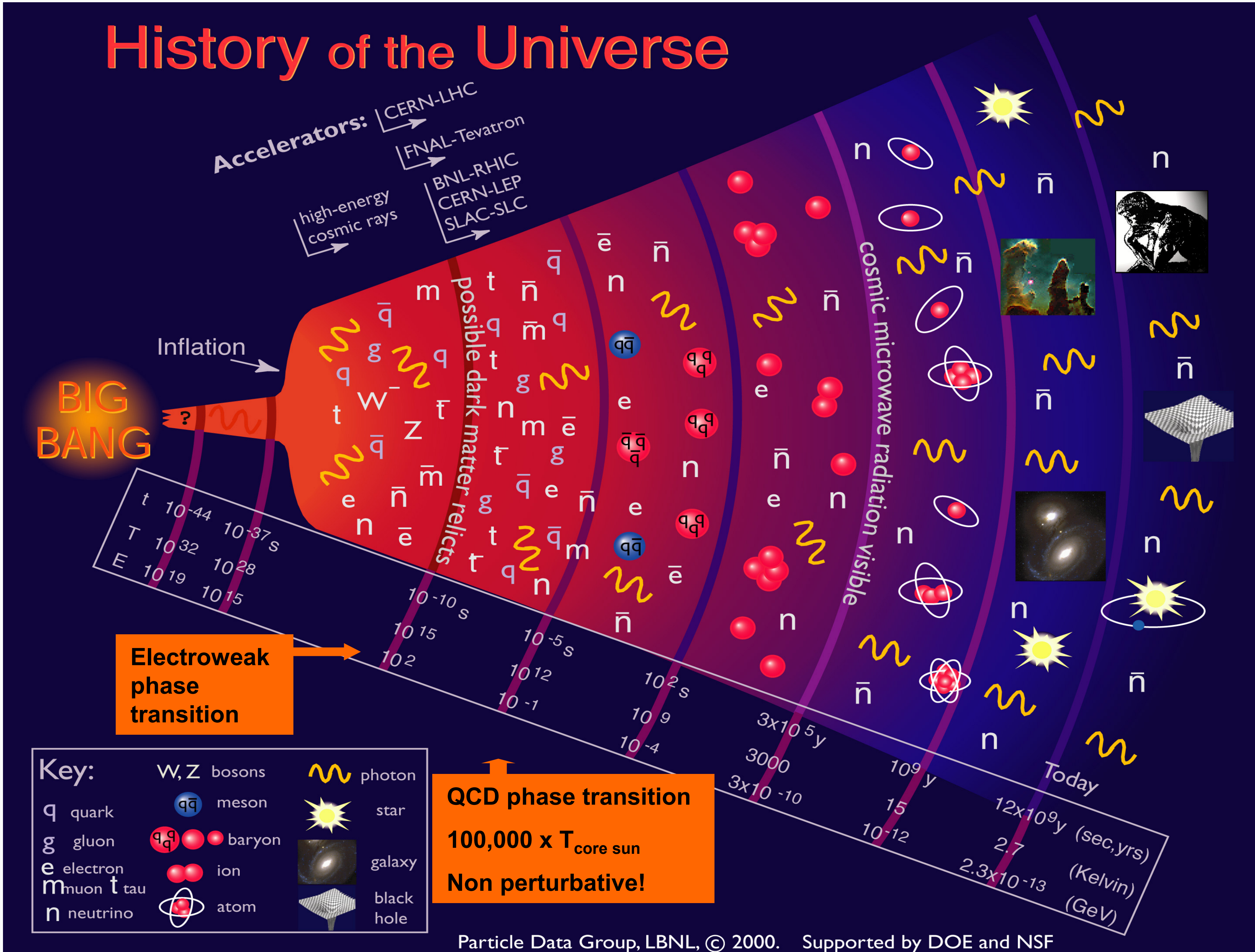

Electroweak phase transition

QCD phase transition

100,000 x $T_{core\ sun}$

Non perturbative!

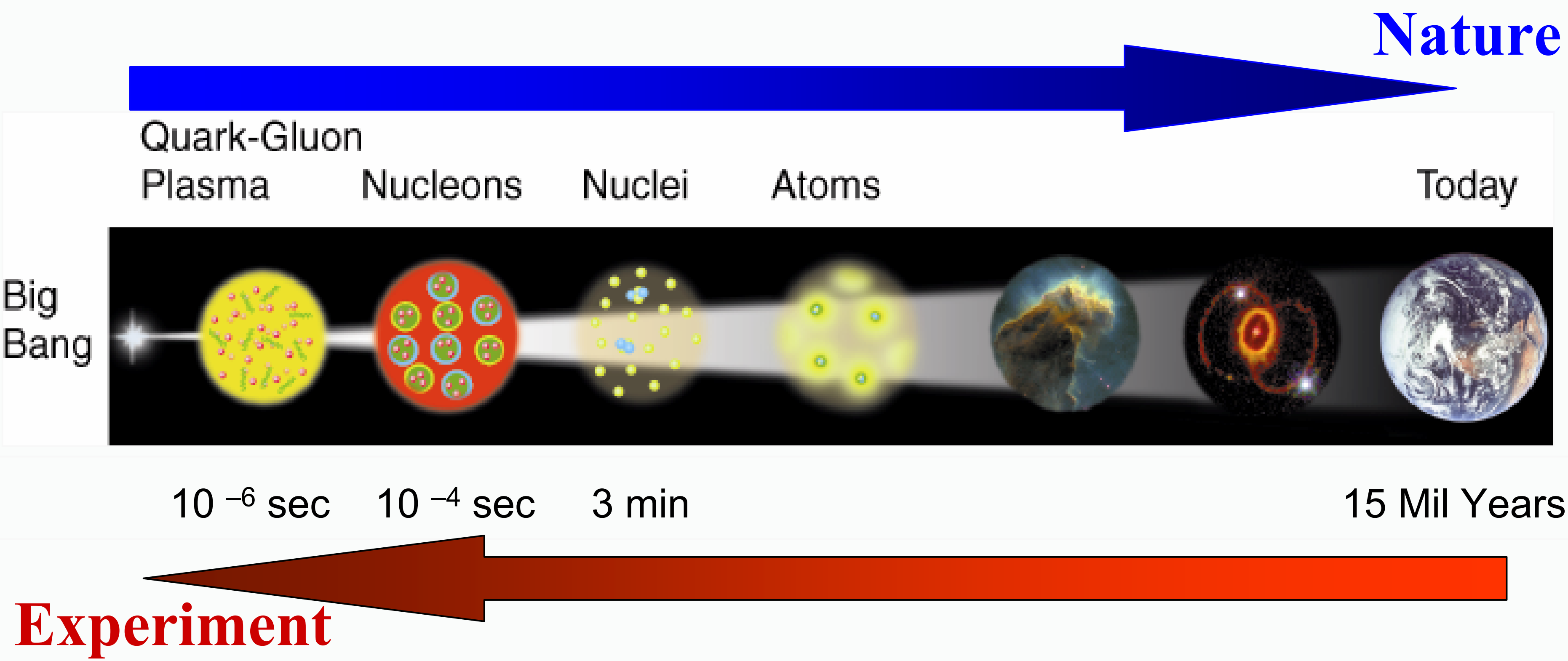
Nature
Quark-Gluon Plasma
Nucleons
Nuclei
Atoms
Today
Big Bang
10 −6 sec
10 −4 sec
3 min
15 Mil Years
Experiment

QGP in the laboratory

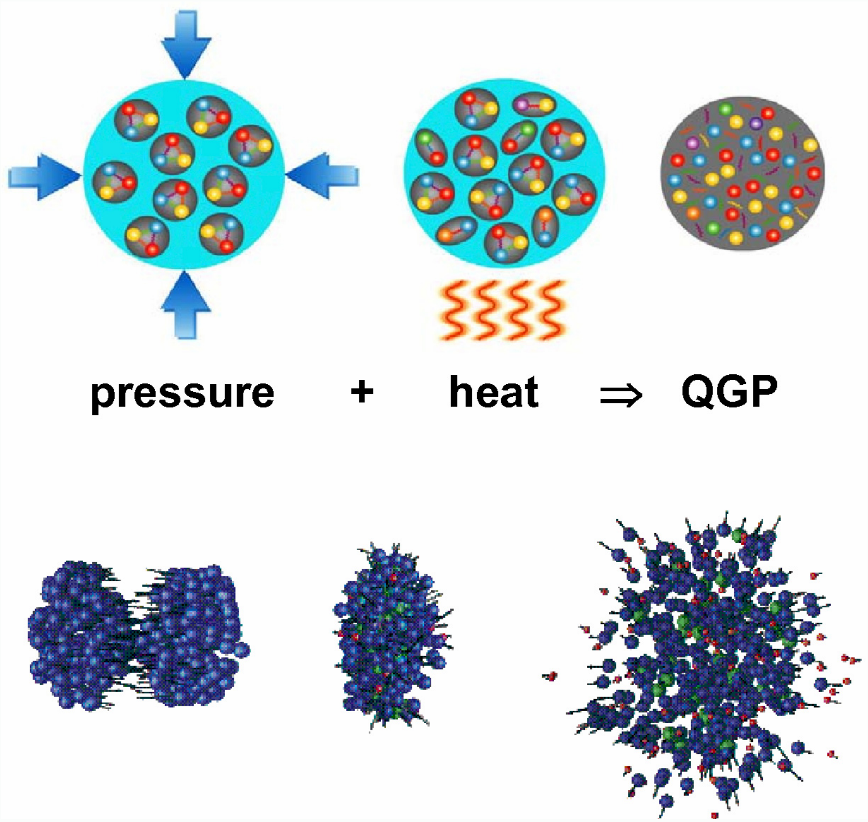

Key parameters: Bombarding energy and collision centrality

Heavy Ion Time Evolution

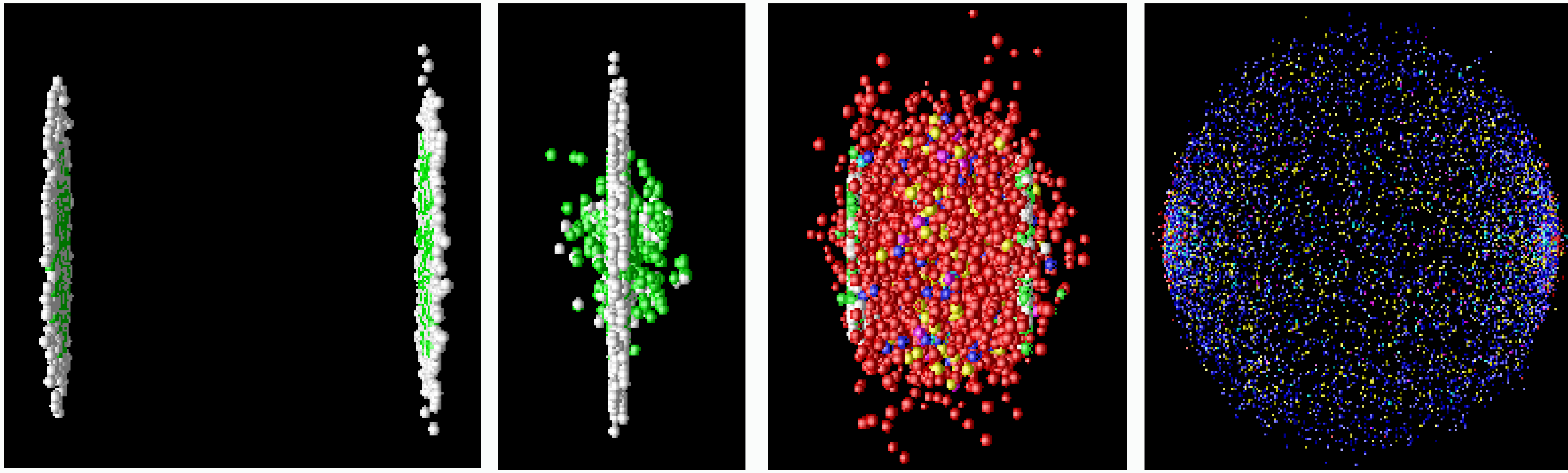

1. Initial Nuclei Collide
2. Partons are Freed from Nuclear Wavefunction
3. Partons interact and potentially form a Quark-Gluon Plasma
4. System expands and cools off
5. System Hadronizes and further Re-Scatters
6. Hadrons and Leptons stream towards our detectors

Onion-like structure of HEP experiments

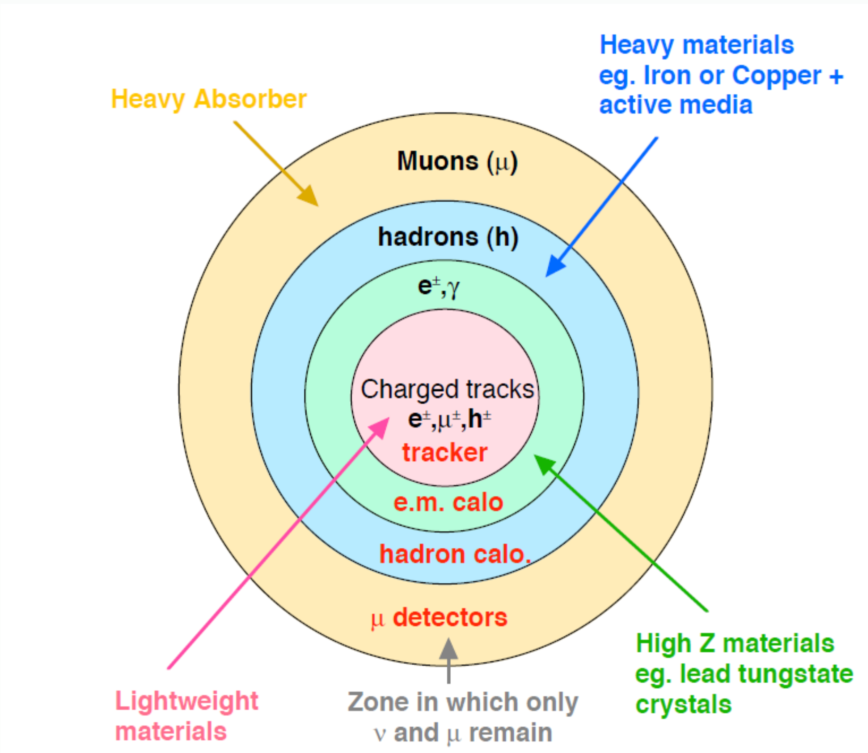

Each layer identifies and measures (or remeasures) the energy of particles unmeasured by the previous layer

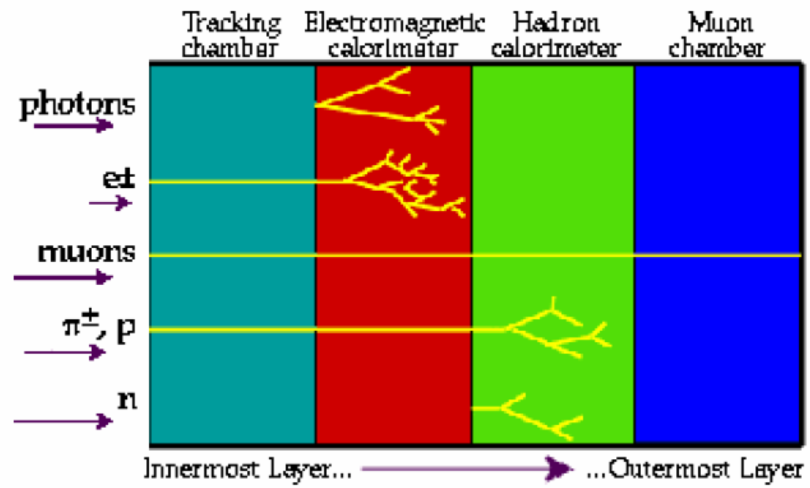

Available energy √s for Fixed Target and Collider experiments

Fixed Target experiment:

m_1, E_1^{lab} ● ⟶ ● $m_2, p_2^{lab} = 0$

$$\sqrt{s} = \sqrt{m_1^2 + m_2^2 + 2E_1^{lab} m_2} \approx \sqrt{2E_1^{lab} m_2}$$

$E_1^{lab} >> m_1, m_2$

Collider experiment:

m_1, E_1^{lab} ● ⟶ ⟵ ● m_2, E_2^{lab}

$$\sqrt{s} = \sqrt{m_1^2 + m_2^2 + 2E_1^{lab} E_2^{lab} + 2 p_1^{lab} p_2^{lab}} = 2E_1^{lab}$$

$\bar{p}_1 = -\bar{p}_2$

$m_1 = m_2$

Kinematics, notations, conventions

c=ħ=1

ħc=197.3269631 MeV.fm

$$\frac{1eV}{k_B} = \frac{1.60217653(14)\times 10^{-19} J}{1.3806505(24)\times 10^{-23} J/K} = 11604.505(20)K$$

$$y = \frac{1}{2}\ln\left(\frac{E+p_z}{E-p_z}\right) = \tanh^{-1}\left(\frac{p_z}{E}\right) \underset{p>>m}{\approx} -\ln\tan\left(\frac{\theta}{2}\right)$$

$$E = m_T \cosh y$$

$$p_x, p_y, p_z = m_T \sinh y$$

$$m_T = \sqrt{m^2 + p_x^2 + p_y^2}$$

$$y = \frac{1}{2}\ln\left[\frac{\sqrt{p_T^2\cosh^2\eta + m^2} + p_T\sinh\eta}{\sqrt{p_T^2\cosh^2\eta + m^2} - p_T\sinh\eta}\right]$$

$$\eta = \frac{1}{2}\ln\left[\frac{\sqrt{p_T^2\cosh^2 y - m^2} + m_T\sinh y}{\sqrt{p_T^2\cosh^2 y - m^2} - m_T\sinh y}\right]$$

$$\frac{dN}{d\eta dp_T} = \sqrt{1 - \frac{m^2}{m_T^2\cosh^2 y}}\frac{dN}{dy dp_T}$$

Pb+Pb collision at LHC at $\sqrt{s}_{NN}$=2.76TeV

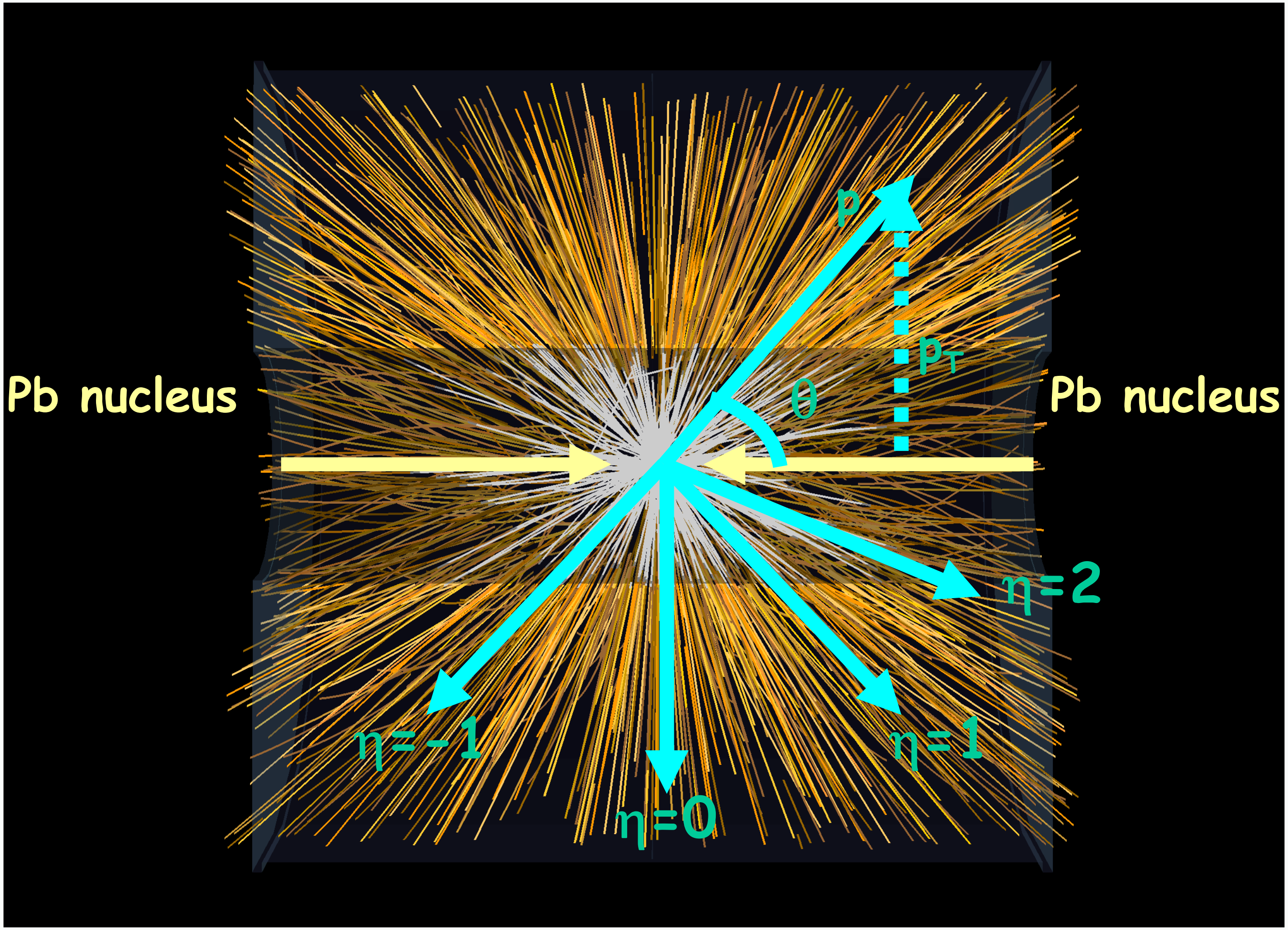

History of Heavy Ion Collisions

- Bevalac (LBL)
  - fixed target (1975-1986) √s <2.4 GeV
- SIS (GSI)
  - fixed target (1989-) √s <2.7 GeV
- AGS (BNL)
  - fixed target (1986-1998) √s <5 GeV
- SPS (CERN)
  - fixed target (1986-2003) √s <20 GeV
- RHIC (BNL)
  - collider (2000-) √s <200 GeV
- LHC (CERN)
  - collider (2008-) √s <5500 GeV
- FAIR (GSI)
  - fixed target (2014-) √s <9 GeV

"Livingston plot"
J. Schukraft nucl-ex/0602014

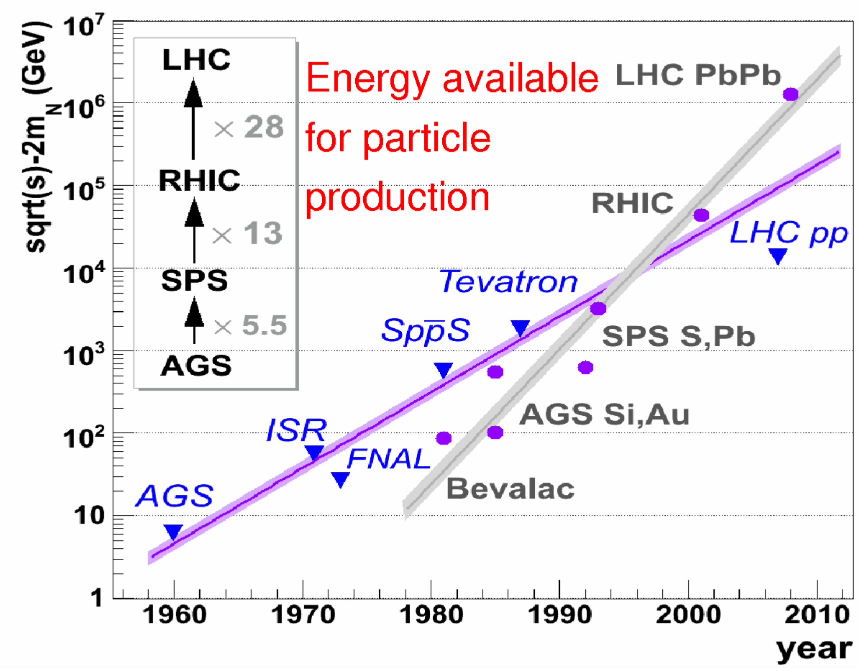

Energy doubling every ~4 (1.7) years for p (ion) beams.

Heavy ion collisions at LHC

	SPS	RHIC	LHC
$\sqrt{s_{NN}}$ (GeV)	17	200	2760(5500)
dN_{ch}/dy	430	730	1584
τ^0_{QGP} (fm/c)	1	0.2	0.1
T/T_c	1.1	1.9	3.0-4.7
ε (GeV/fm^3)	3	5	>18
τ_{QGP} (fm/c)	≤2	2-4	≥10
τ_f (fm/c)	~10	20-30	15-60
V_f(fm^3)	few 10^3	few 10^4	few 10^5

faster
hotter
denser
longer

bigger

LHC: Entering a new regime

C W Fabjan 2008 J. Phys. G: Nucl. Part. Phys. 35, 104038

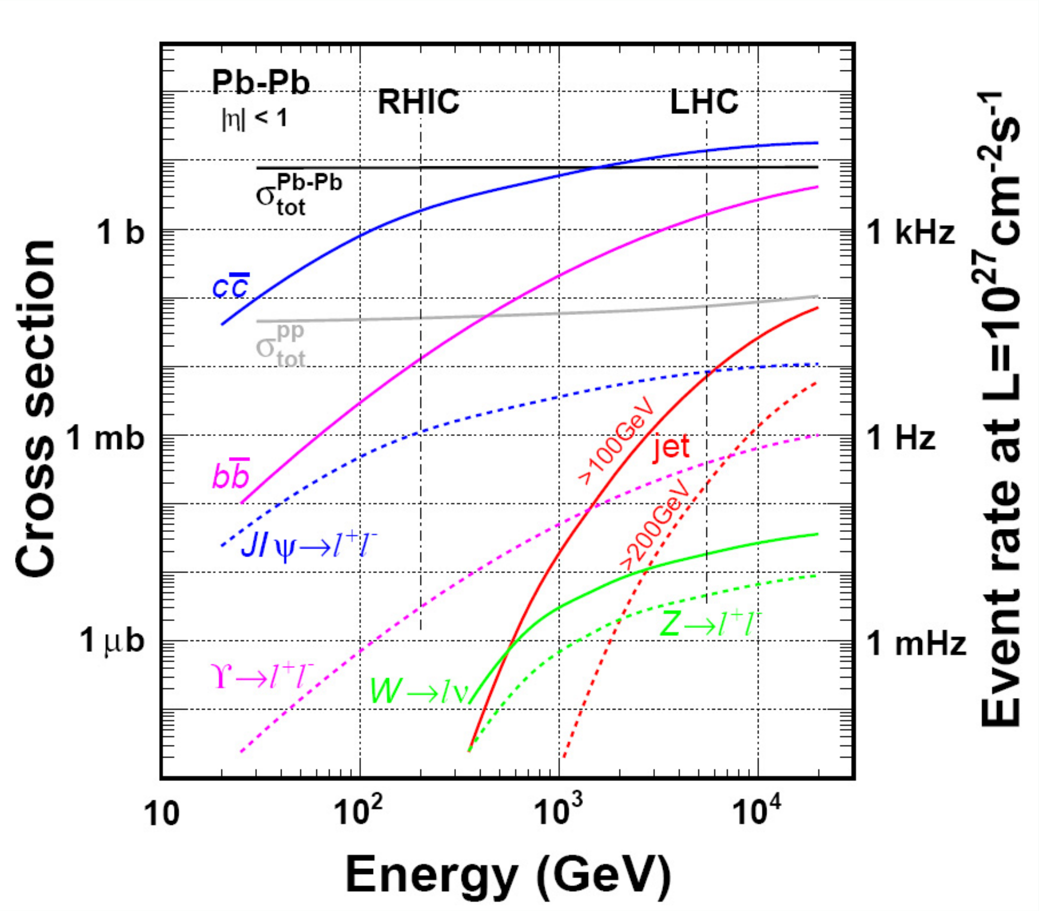

Cross-sections of interesting probes expected to increase by factors
~ 10 ($c\bar{c}$) to
$\sim 10^2$ ($b\bar{b}$) to
$\sim > 10^5$ (very high p_T jets) ;
Hard probes of the medium accessible at LHC
Direct photons are abundantly produced at LHC

THE LHC

The CERN accelerator complex

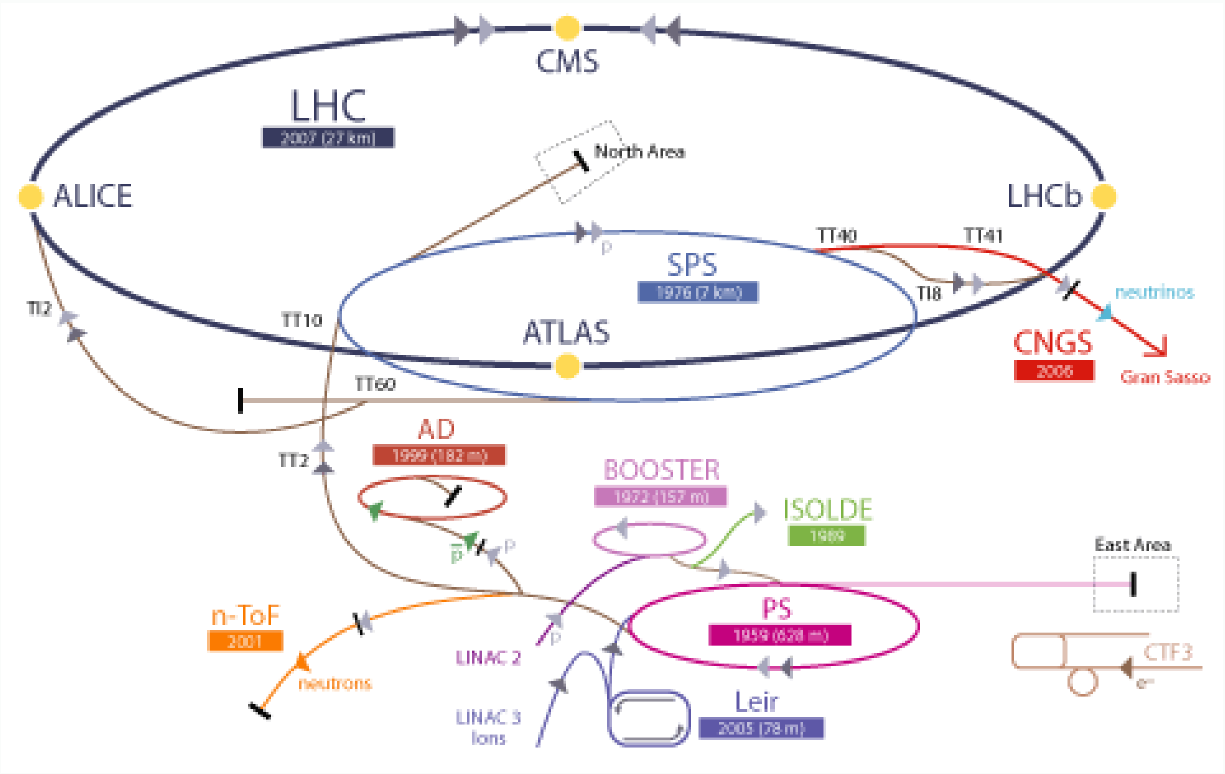

LINAC2- BOOSTER-PS-SPS-LHC

LHC startup

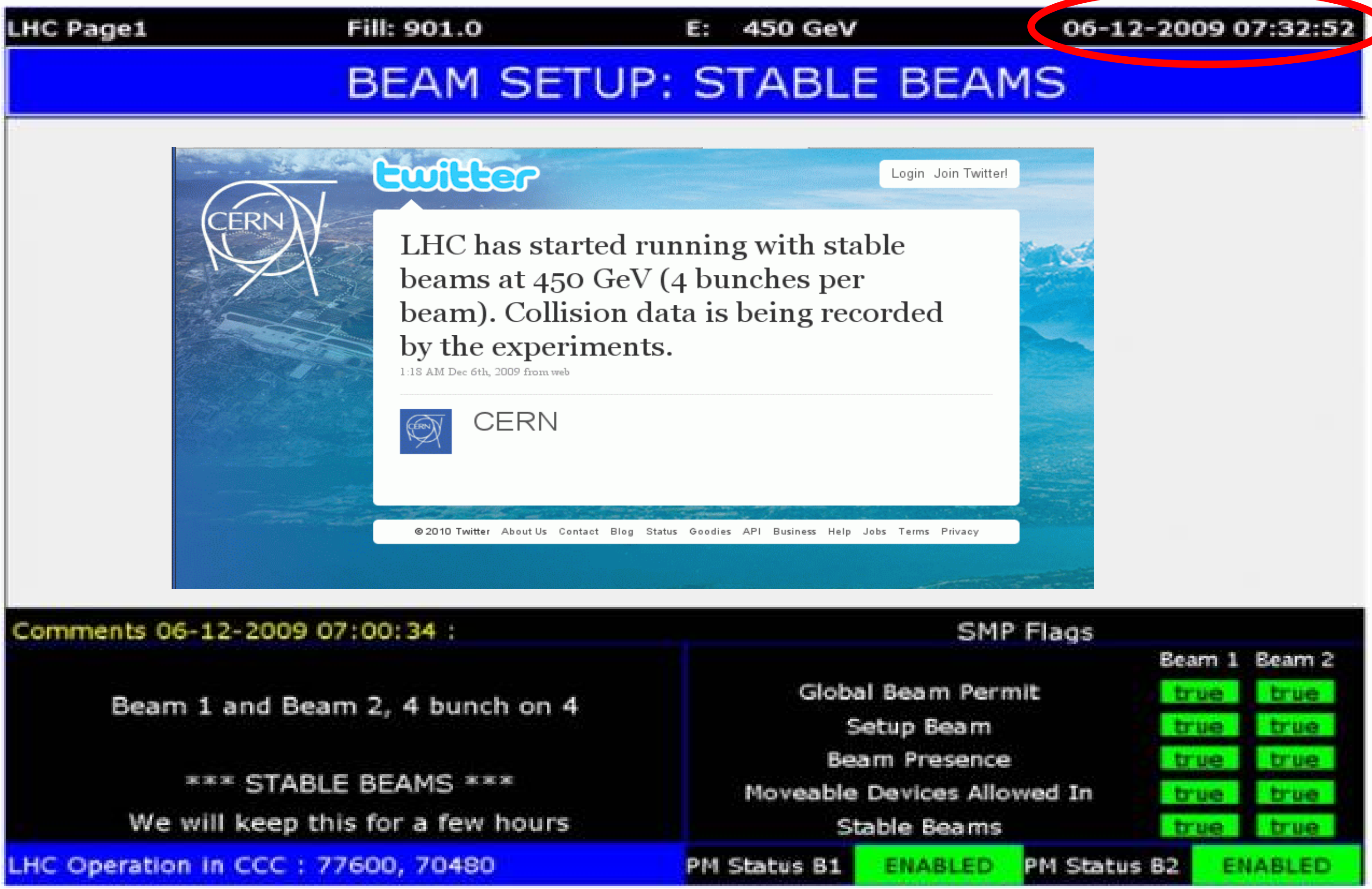

LHC Page1
Fill: 901.0
E: 450 GeV
06-12-2009 07:32:52
BEAM SETUP: STABLE BEAMS
twitter
Login Join Twitter!
CERN
LHC has started running with stable beams at 450 GeV (4 bunches per beam). Collision data is being recorded by the experiments.
1:18 AM Dec 6th, 2009 from web
CERN
© 2010 Twitter About Us Contact Blog Status Goodies API Business Help Jobs Terms Privacy
Comments 06-12-2009 07:00:34 :
Beam 1 and Beam 2, 4 bunch on 4
*** STABLE BEAMS ***
We will keep this for a few hours
SMP Flags
Beam 1 Beam 2
Global Beam Permit true true
Setup Beam true true
Beam Presence true true
Moveable Devices Allowed In true true
Stable Beams true true
LHC Operation in CCC : 77600, 70480
PM Status B1 ENABLED
PM Status B2 ENABLED

The Large Hadron Collider

- 27 km de circumference
- 40-100 m underground
- 1232 super conducting magnets
15 m long 30Tons.
- Cooled at 1.9 K (liquid He)

- Accelerates p @ 7×10^{12} eV and ions @ $2{,}76\times10^{12}\times A$ eV (99,999993% c)
- Luminosity from 10^{33} to 10^{27} $cm^{-2}s^{-1}$ (depeding on the beams and experiment)
- Bunches of ~10^{8} ions cross each other 10^{7} times per second to make 8000 ion-ion collisions per second
- Up to $0{,}2\times10^{-3}$ Joules available in a collision

The Large Hadron Collider

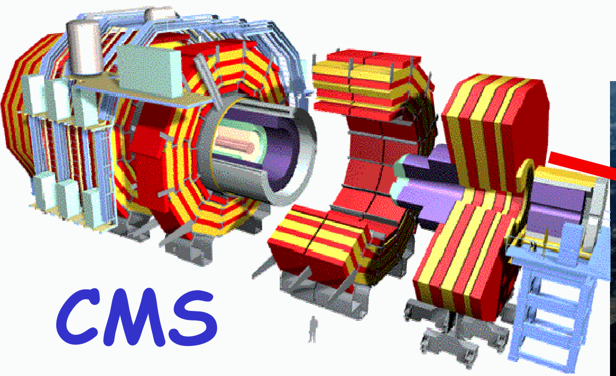

CMS

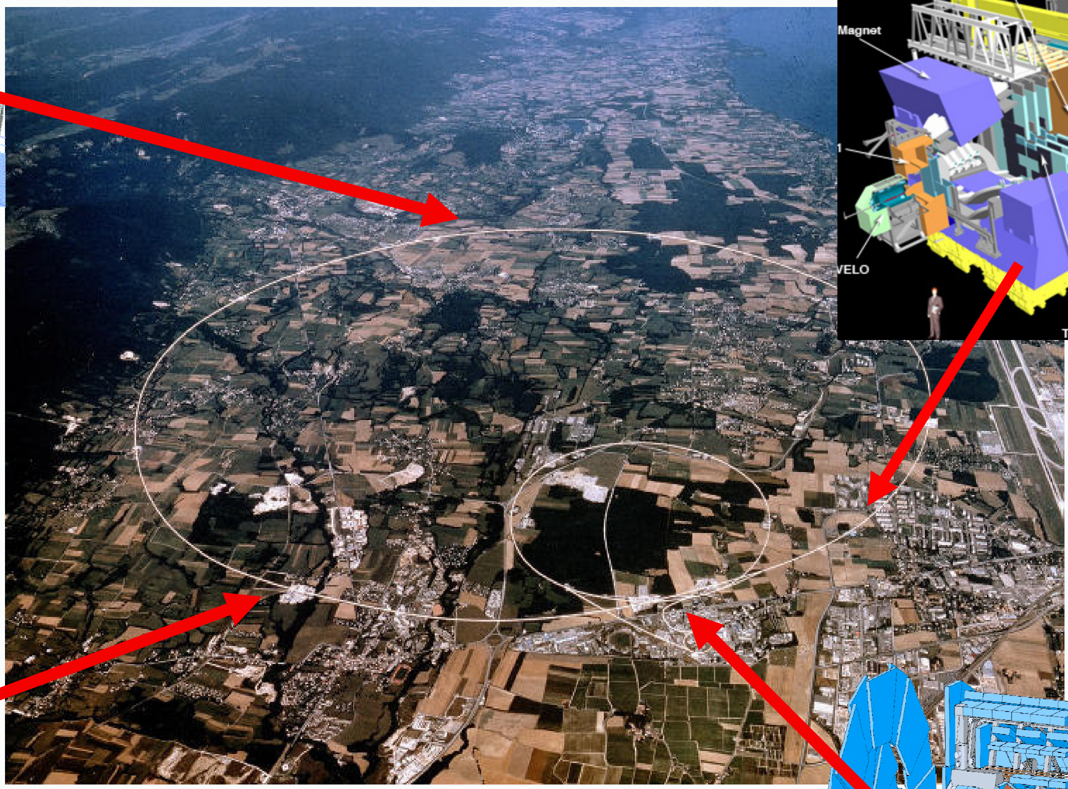

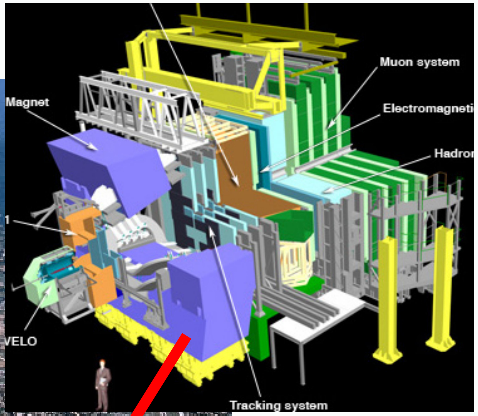

LHCb

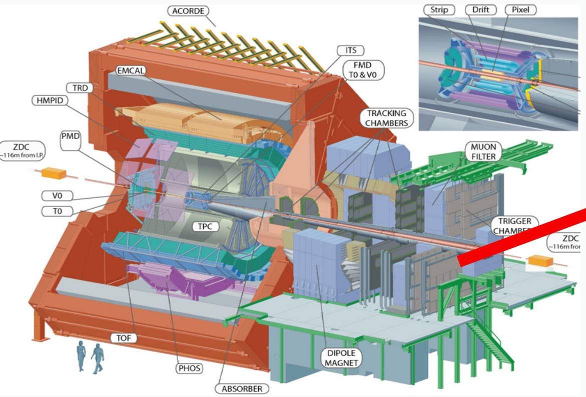

ALICE

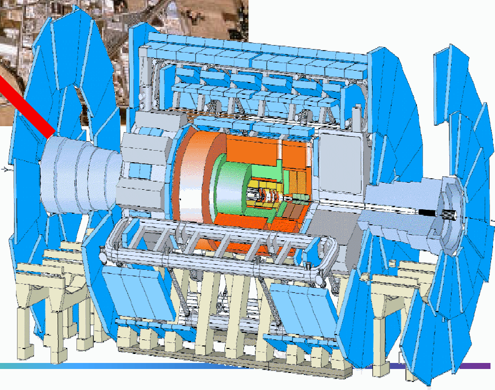

ATLAS

The ATLAS Detector

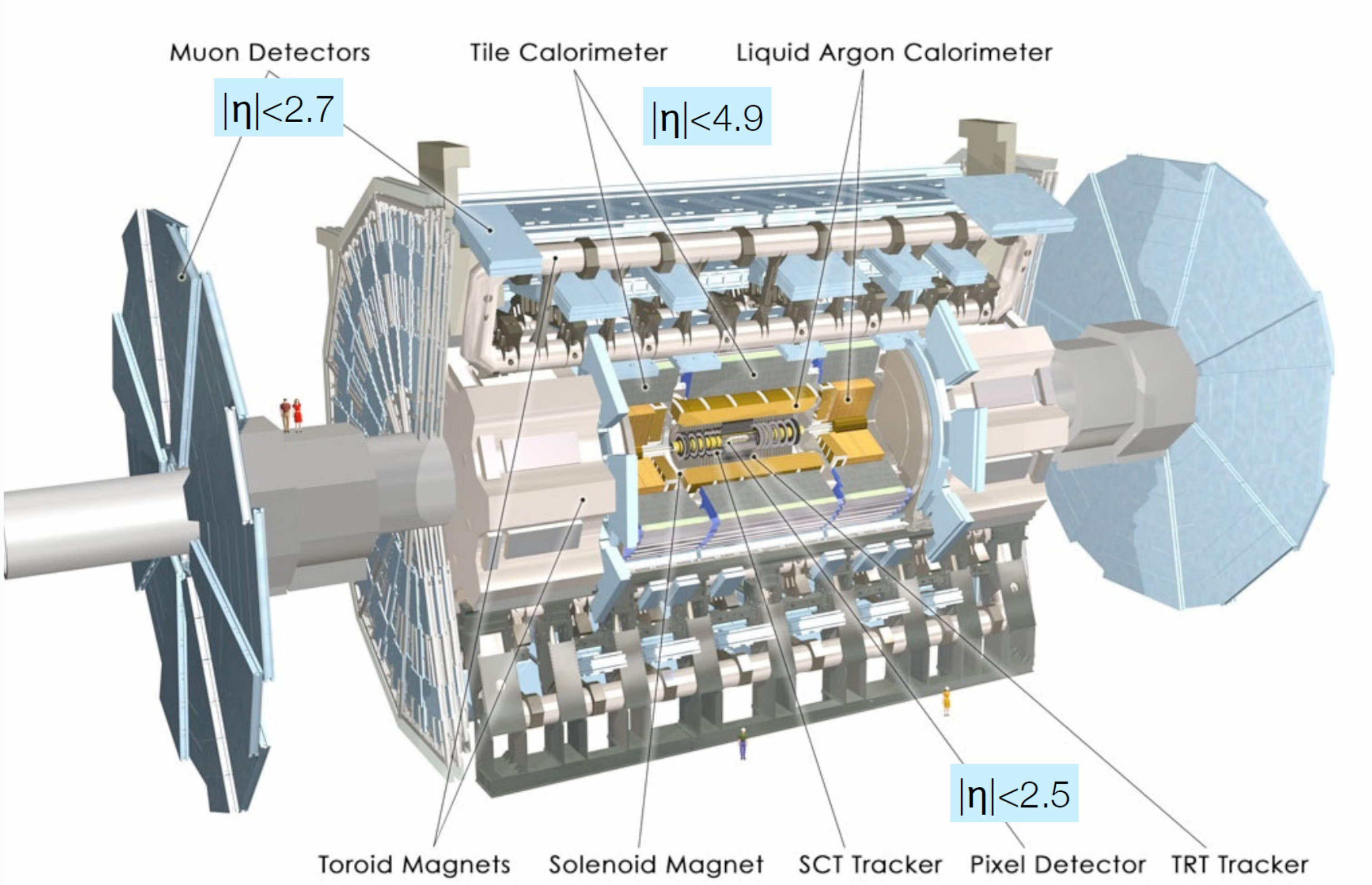

The CMS experiment

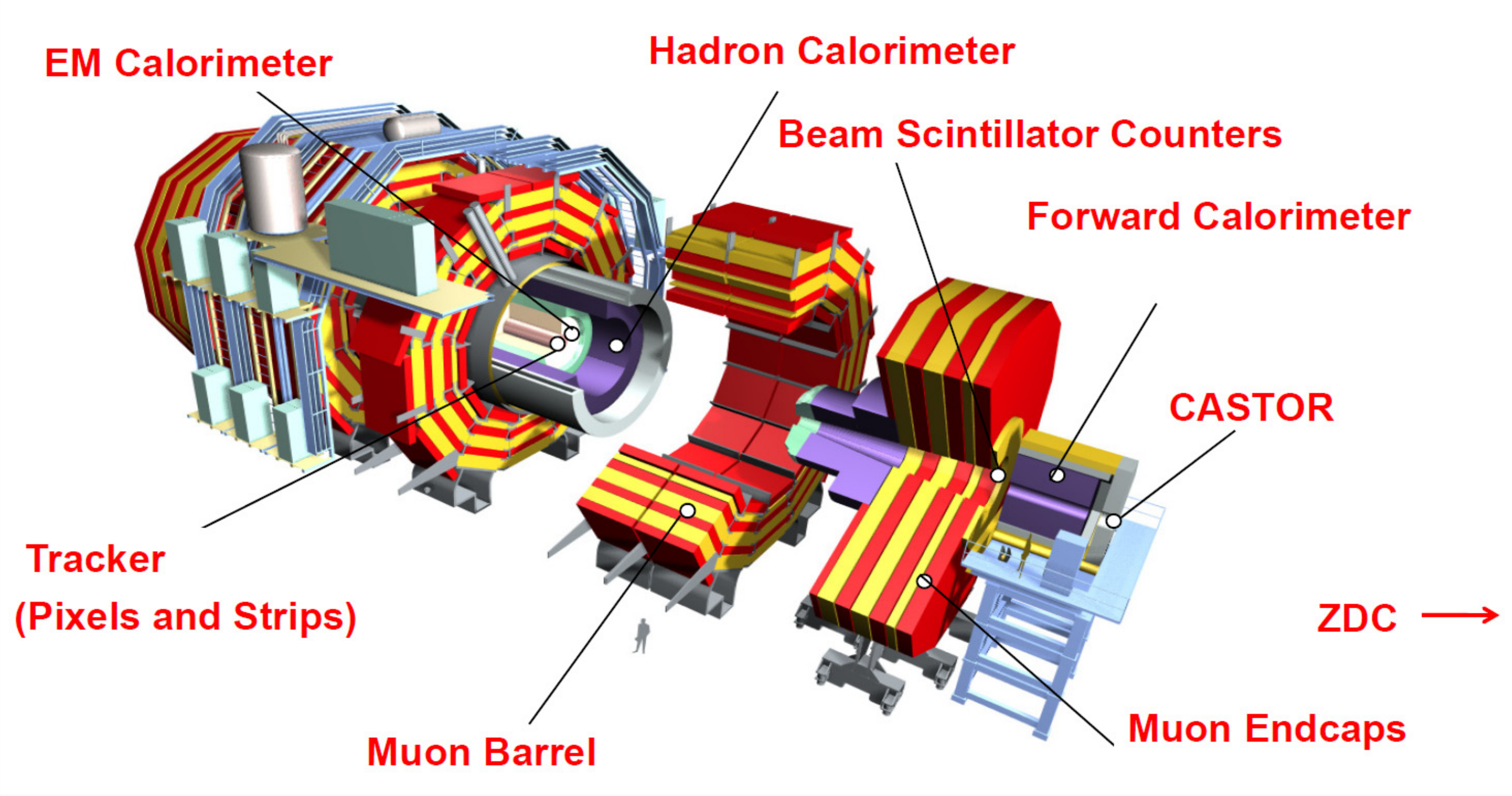

The ALICE Experiment

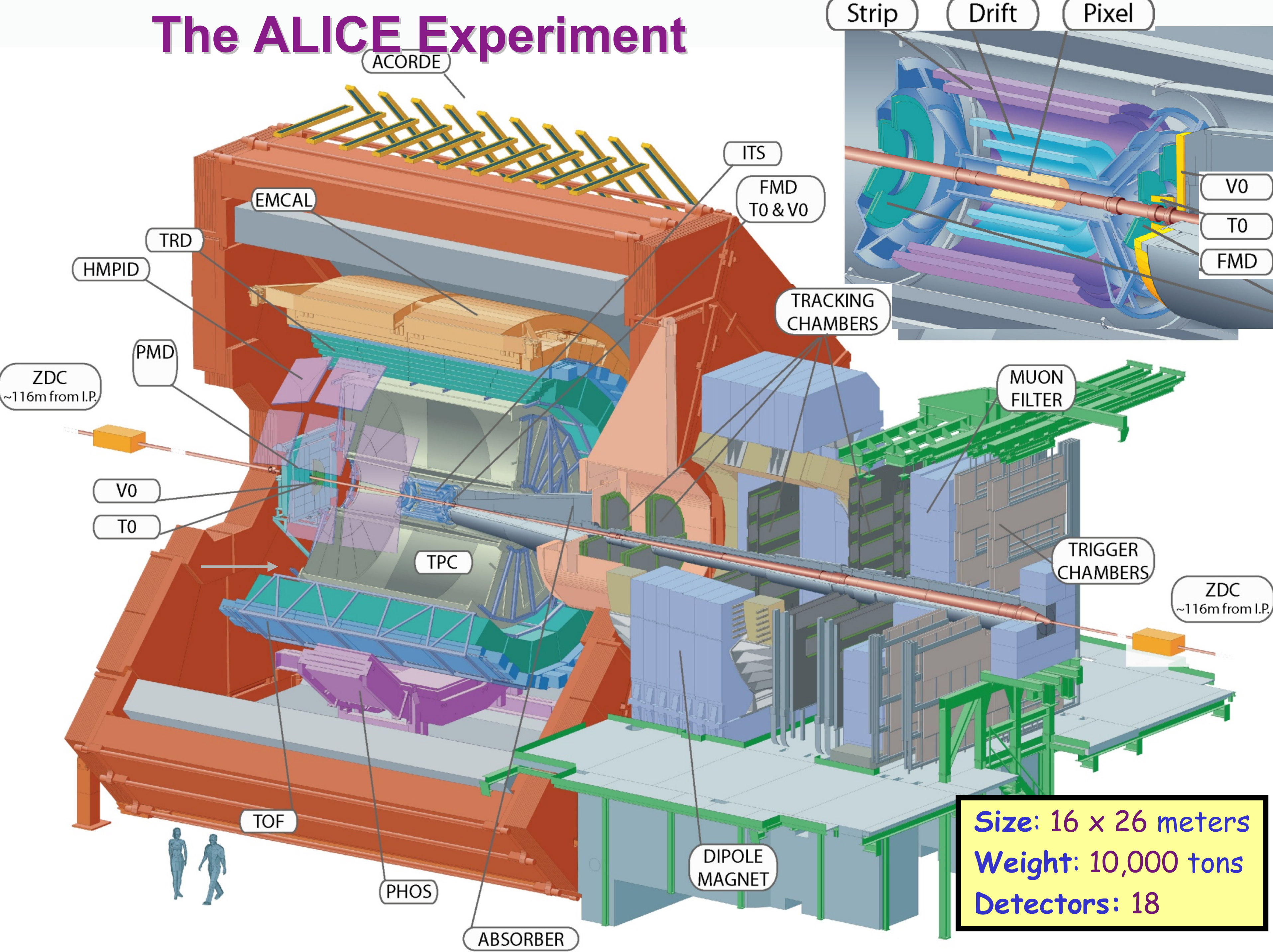

Size: 16 x 26 meters
Weight: 10,000 tons
Detectors: 18

PID in ALICE

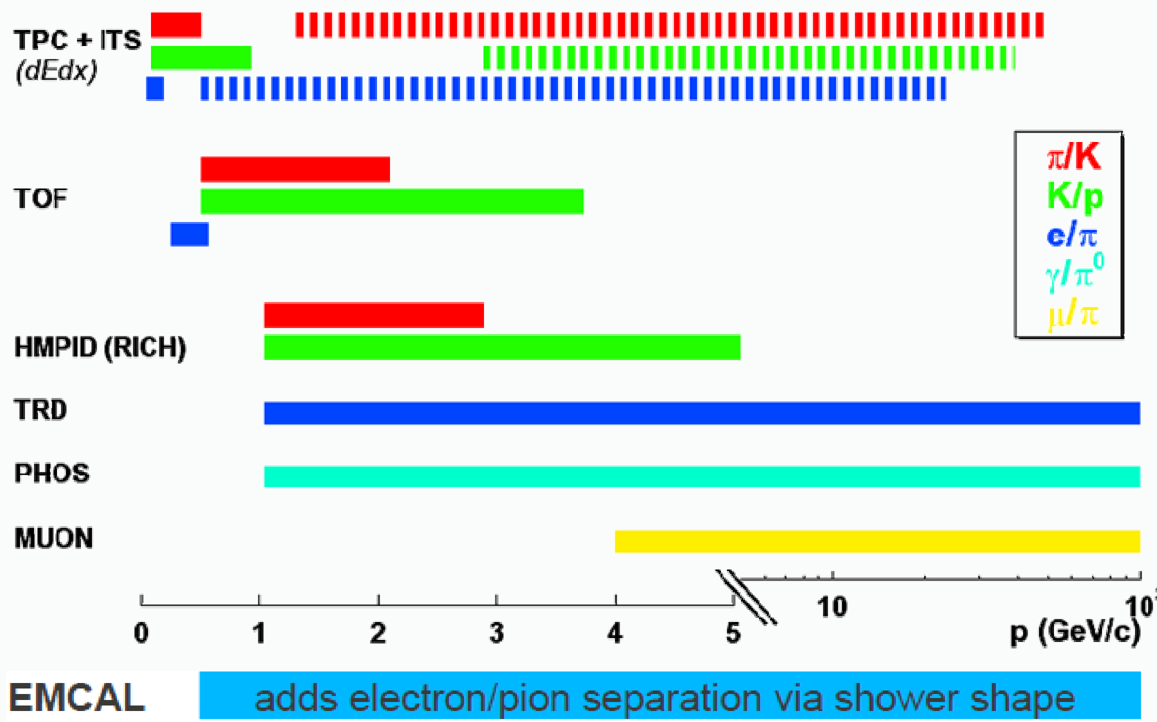

•excellent particle ID up to ~ 50 to 60 GeV/c

•Most (2π * 1.8 units η) of the hadrons (dE/dx + ToF), leptons (dE/dx, TOF, transition radiation) and photons (high resolution EM calorimetry, conversions);

•Track and identify from very low (< 100 MeV/c) up to very high pt (>100GeV/c);

•Identify short lived particles (hyperons, D/B meson) through secondary vertex detection;

Collision picture

Landau versus Bjorken scenario

Figure: *Nuclear stopping scenarios. The particle rapidity distributions are given before the collision and after the collision in the case of a full stopping (Landau) and complete transparency (Bjorken).*

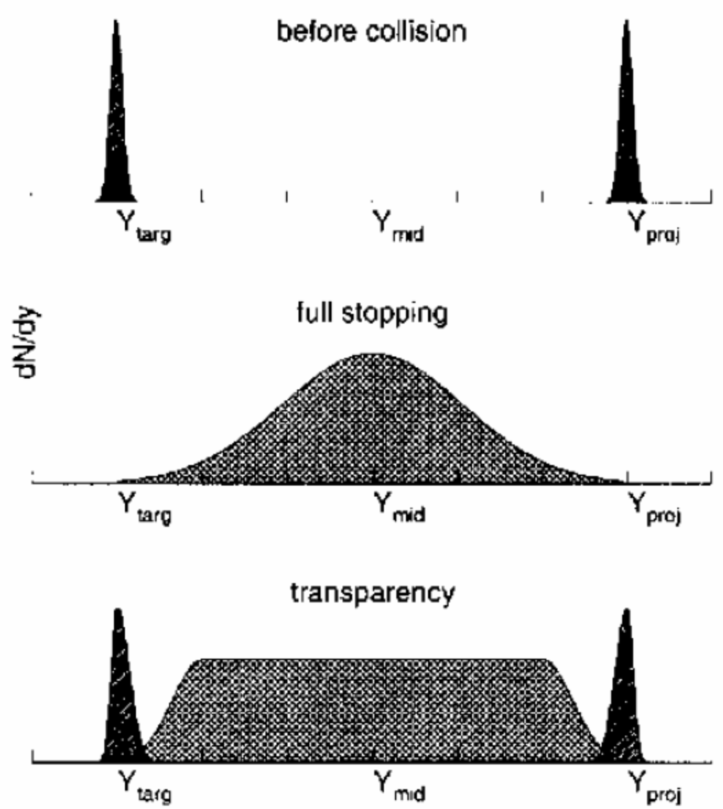

www-subatech.in2p3.fr/~photons/subatech/physics/potpourri/node11.html

Landau:

L.D. Landau, Izv. Akad. Naul. SSSR, Ser. Fiz. 17(1953) 51

- Complete stopping of the nuclei
- Initial conditions:

$V_0 = V_{rest}/\gamma_{cm}, \quad \varepsilon_0 = E_{cm}/V_0$

- Linear expansion until size comparable to transverse size, then transverse expansion considered
- dN/dy Gaussian with width given by:

$$\sigma^2 = \ln\left(\frac{\sqrt{s}}{2m_p}\right)$$

Bjorken:

- Transparency
- Flat rapidity distribution

Complete stopping of the nuclei in central collisions up to $\sqrt{s}_{NN}$ ~ 5 - 10 GeV,
Transparency (baryon-free QGP at central rapidities) for $\sqrt{s}_{NN}$ > ~ 100 GeV

The Bjorken model and energy density

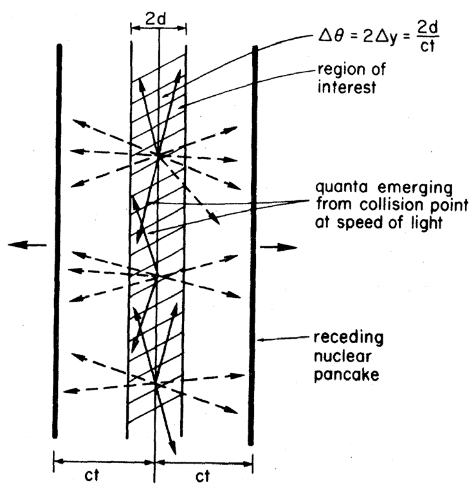

FIG. 2. Geometry for the initial state of centrally produced plasma in nucleus-nucleus collisions.

Phys. Rev. D 27(1983)140

Based on the observation that rapidity distribution of charged secondaries is constant in the mid-rapidity region in a p+p collision. Energy density is also constant. Density of charged particles depend on the proper time τ

$$n_{ch} = n_{ch}(t,z) = n_{ch}(\tau)$$

$$\tau = t/\gamma = t\sqrt{1-v^2} = \sqrt{t^2 - z^2}$$

$$v = z/t = \tanh(y)$$

$$z = \tau \sinh y$$

$$t = \tau \cosh y$$

$$\frac{\Delta N}{A\Delta z} = \frac{1}{A}\frac{dN}{dy}\frac{dy}{dz}\Big|_{y=0}$$

$$= \frac{1}{A}\frac{dN}{dy}\frac{1}{\tau_o \cosh y}\Big|_{y=0}, where$$

$$dz = \tau \cosh y dy$$

$$\varepsilon_0 = m_T \cosh y \frac{\Delta N}{A\Delta z}$$

$$\boxed{\varepsilon_o = \frac{m_T}{\tau_o A}\frac{dN}{dy}\Big|_{y=0} = \frac{1}{\tau_o A}\frac{dE_T}{dy}\Big|_{y=0}}$$

Centrality, participants, expectators

N. Herrmann, J.P. Wessels, T. Wienold, Ann. Rev. Nucl. Part. Sci 49 (1999) 581

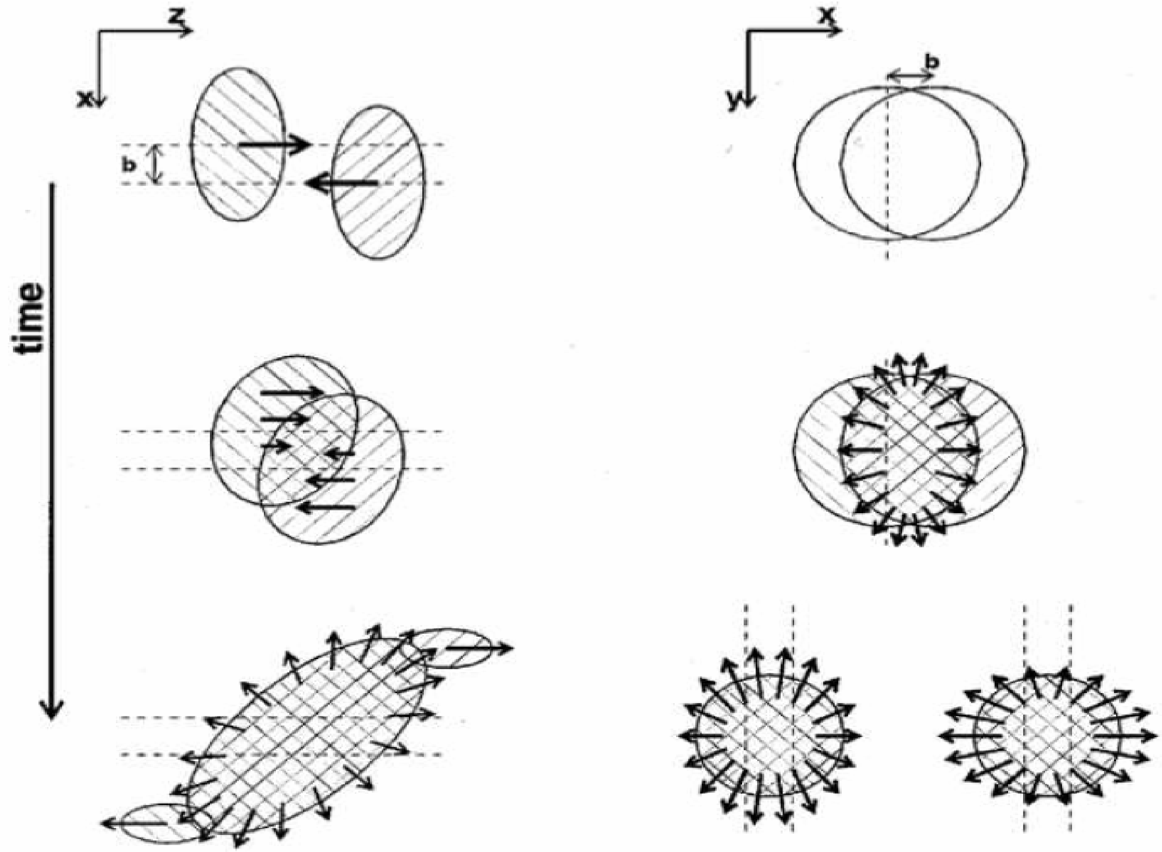

Impact parameter b:
a 2D vector connecting the centers of the 2 nuclei; points in x direction.

Central collisions: small b
Peripheral collisions: large b

Participants: nucleon that may hit each other
Spectators: do not meet any other nucleon in their way

Glauber model

Glauber, RJ. 1959. In *Lectures in Theoretical Physics*, ed. WE Brittin and LG Dunham, 1:315. New York:Interscience

- Relates the impact parameter to N_{coll} and N_{part}
- Geometrical model: Assumption of constant inelastic cross section σ_{inel} for each subsequent collision
- Input nuclear density: Woods-Saxon, ...

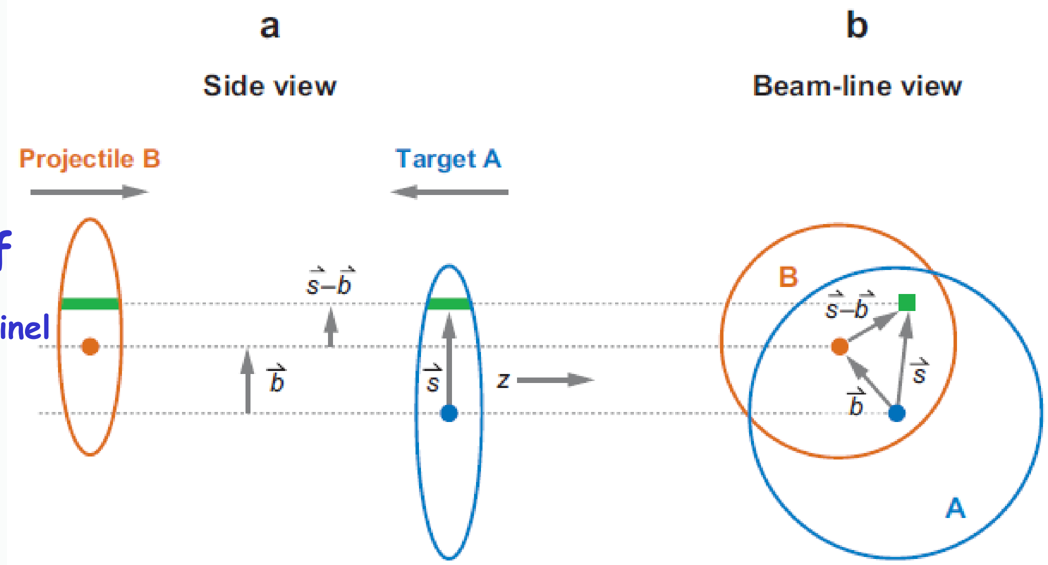

Fig. from Annu. Rev. Nucl.Part.Sci 2007.57:205

Nuclear thickness function: $$T_A(b) = \int dz \rho_A(b,z) \qquad \int d^2b T_A(b) = A$$

Nuclear overlap function: $$T_{AB}(b) = \int d^2s T_A(s) T_B(|\vec{b}-\vec{s}|) \qquad \int d^2b T_{AB}(b) = AB$$

Glauber model: N_{coll} , N_{part}

Number of nucleon-nucleon collisions: $< N_{coll}(b) >= \sigma_{inel} T_{AB}(b)$

N_{part} in nucleus A proportional to nuclear profile function at transverse position s weighted by the sum over the probability of a nucleon-nucleus collision at transverse position |b̄-s̄| in nucleus B. Same for B. Total:

$$N_{part}(b) = \int d^2s[T_A(s)(1-\exp[-\sigma_{inel} T_B(|\vec{b}-\vec{s}|)]) + T_B(|\vec{b}-\vec{s}|)(1-\exp[-\sigma_{inel} T_A(s)])]$$

Au+Au $\sqrt{s_{NN}}$=200GeV

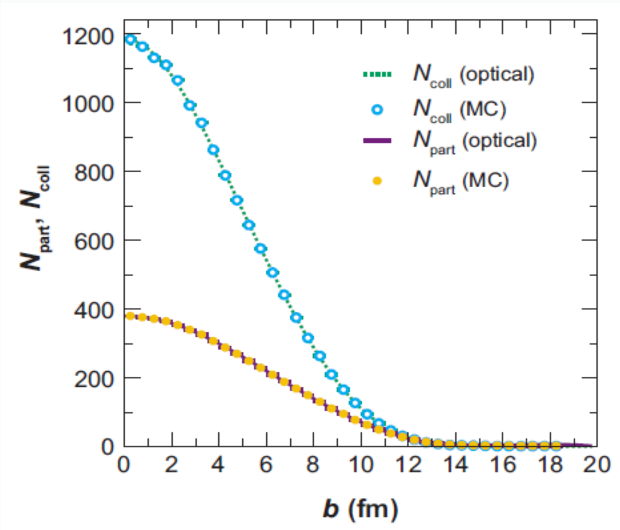

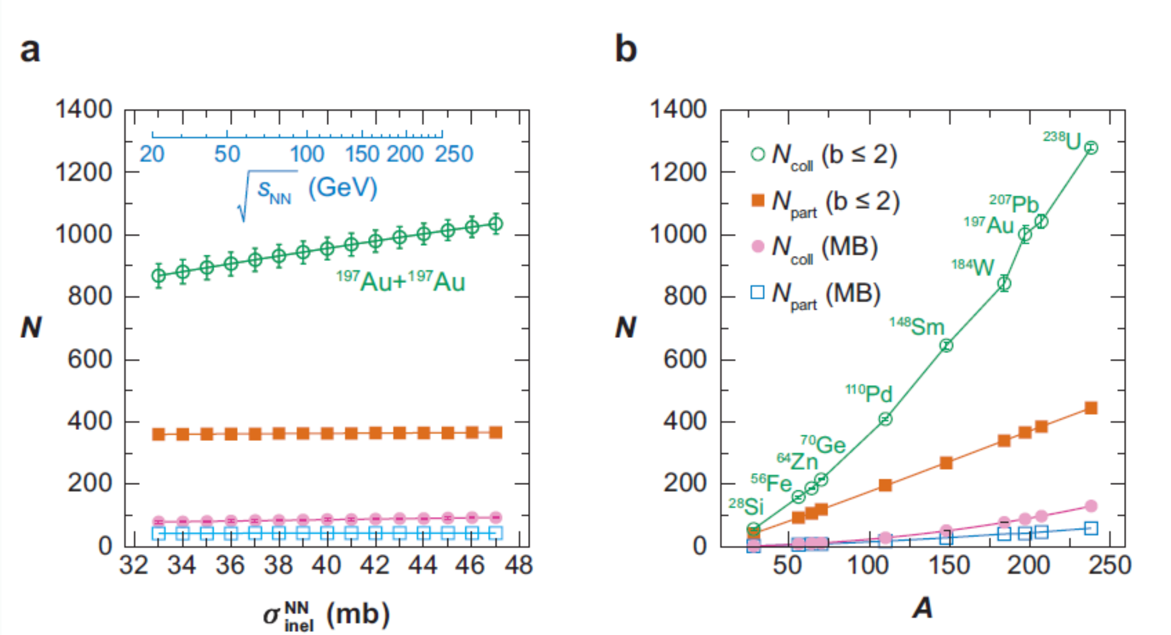

Annu. Rev. Nucl. Part. Sci 2007.57: 205

N_{coll} depends on energy because σ_{inel} grows with $\sqrt{s}$

Centrality at LHC: ALICE

Phys. Lett. B 696 (2011) 30-39,
Phys. Rev. Lett. 106, 032301 (2011)

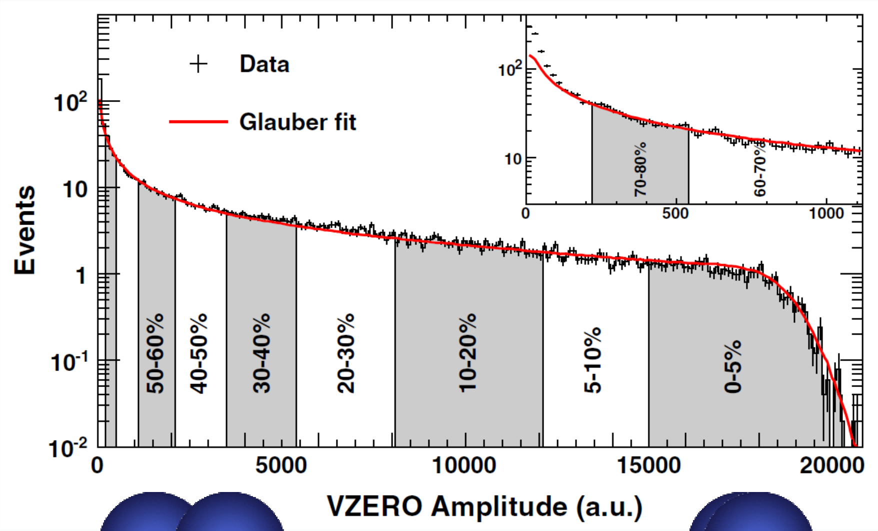

Table 1
The average numbers of participating nucleons $\langle N_{part} \rangle$, binary nucleon–nucleon collisions $\langle N_{coll} \rangle$, and the average nuclear overlap function $\langle T_{AA} \rangle$ for the two centrality bins, expressed in percentages of the hadronic cross section.

Centrality	$\langle N_{part} \rangle$	$\langle N_{coll} \rangle$	$\langle T_{AA} \rangle$ (mb^{-1})
0–5%	383 ± 3	1690 ± 131	26.4 ± 0.5
70–80%	15.4 ± 0.6	15.7 ± 0.7	0.25 ± 0.01

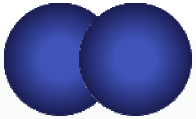

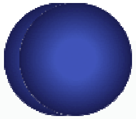

Number of ancestors given by: $f \times N_{part} + (1-f) \times N_{coll}$

Global properties

Nuclear Stopping

F. Videbaek and O. Hansen, Phys. Rev. C 52 (1995)2684

- Baryon number is conserved in the collision
- Quantified by net baryon counting (N_{baryon}-$N_{antibaryon}$)

Lower energies:

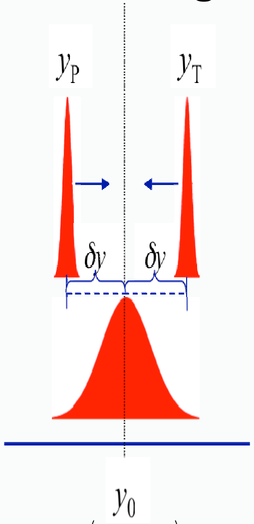

Higher energies:

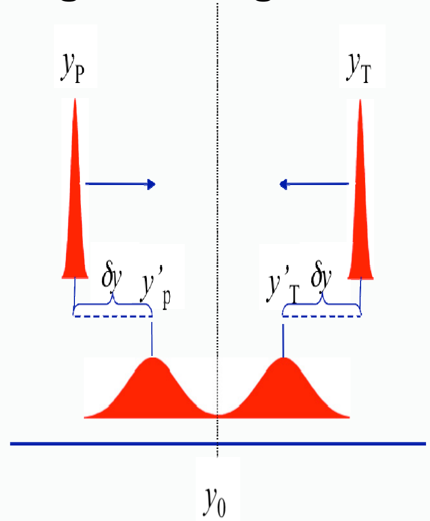

Stopping:
Average rapidity loss of net-baryons
(from net-protons using MC).

$$\langle \Delta y \rangle = y_p - \langle y_{net-b} \rangle,$$

$$\langle y_{net-b} \rangle = \int_o^{y_p} y \frac{dN_{net-b}(y)}{dy} dy$$

$$\langle E_{net-b} \rangle = \frac{1}{N_{part}} \int_o^{y_p} E \frac{dN_{net-b}(y)}{dy} dy \approx \frac{1}{N_{part}} \int_o^{y_p} m \cosh y \frac{dN_{net-b}(y)}{dy} dy, with \langle m_T \rangle \approx m$$

$$E_{inel} = \frac{\sqrt{s_{NN}}}{2} - \langle E_{net-b} \rangle, K = \frac{2E_{inel}}{\sqrt{s_{NN}} - 2m_p}$$

Full stopping: $\langle \Delta y \rangle = y_p$

Transparency: $\langle \Delta y \rangle = 0$

Nuclear Stopping

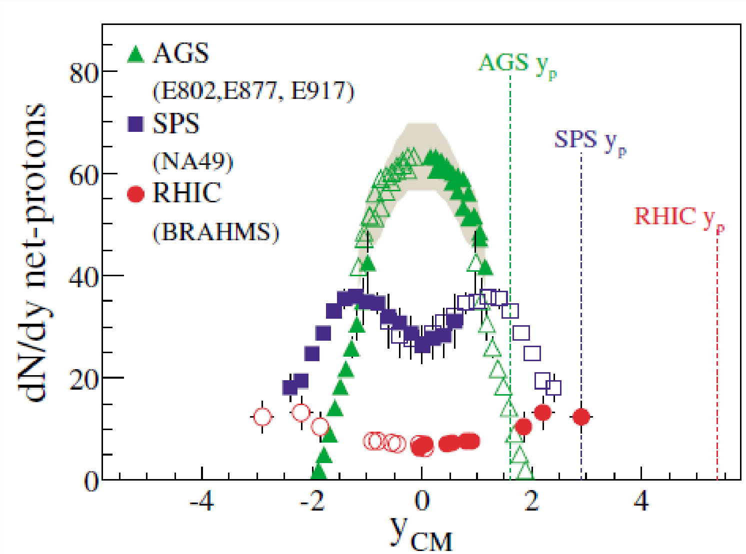

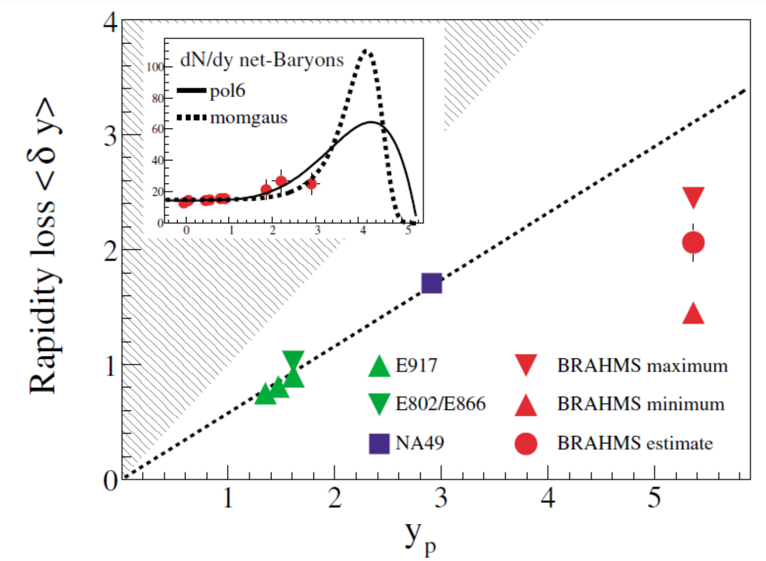

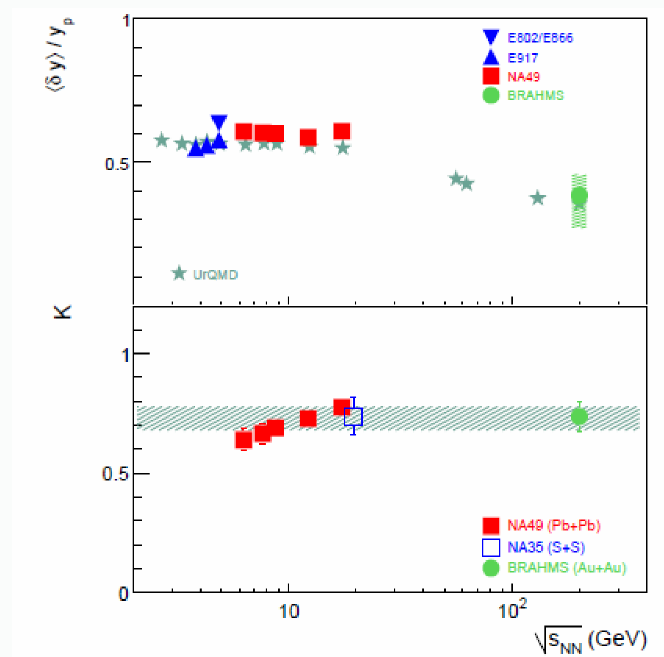

RHIC ($\sqrt{s_{NN}}$ = 200 GeV):

E = 27 ± 6 GeV

E_{inel} = 73.0 ± 6.0 GeV (available for excitations)

BRAHMS: PRL93, 102301 (2004)
J. Phys. G: Nucl. Part. Phys. 34 (2007) S951

Charged particle multiplicity

- Simple observable: just count tracks
- Constraints on the dominant mechanisms of the particle production
- Soft interactions, QCD cannot be applied
  - Input for phenomenological models
- Essential to estimate the initial energy density
- Dependence on $\sqrt{s}$ and on system size interplay between hard parton-parton scattering processes and soft processes

First PbPb collisions in ALICE

0-5% cent: $dN_{ch}/d\eta$ ~ 1584 ± 4 (stat) ± 76 (syst)

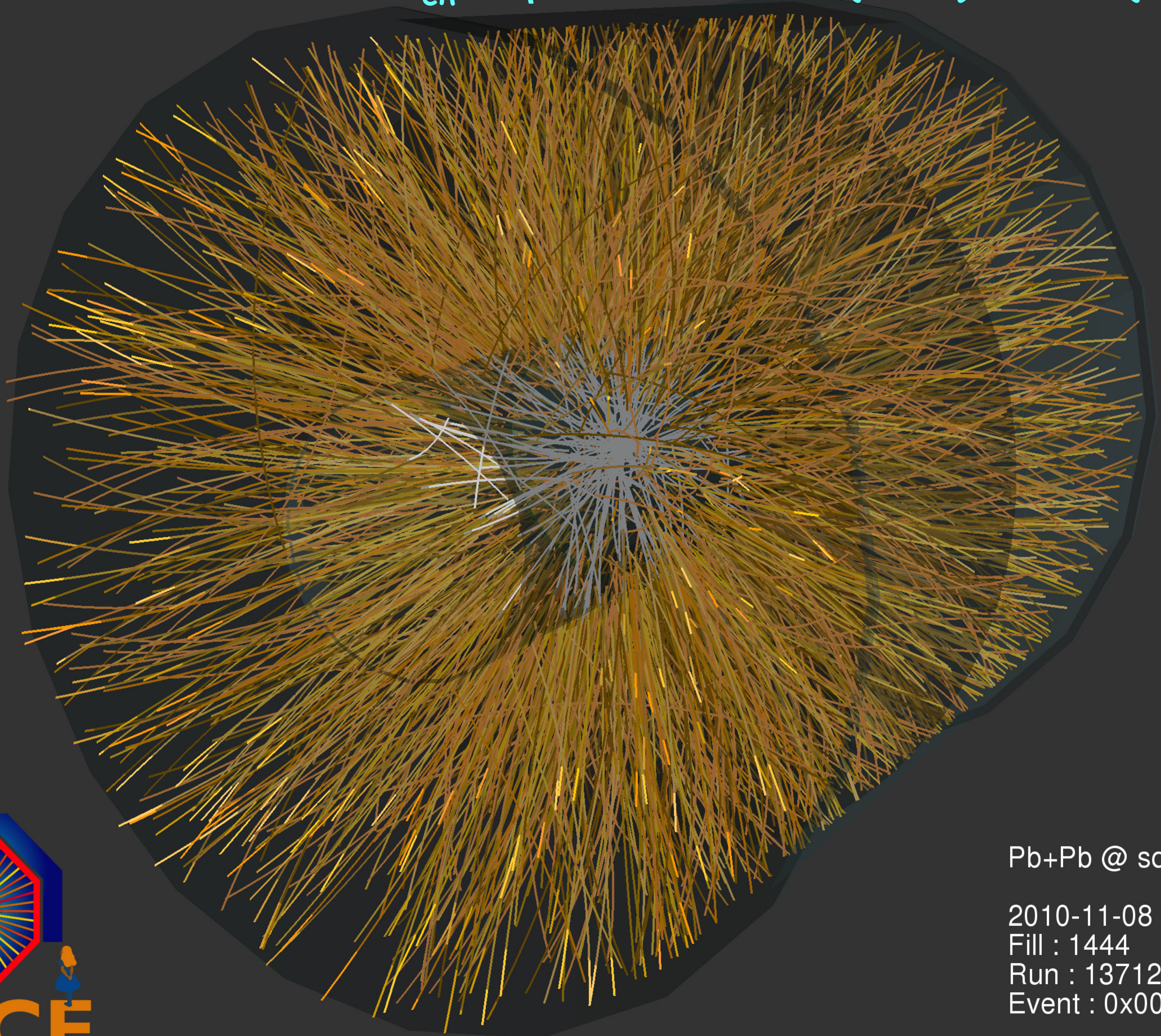

ALICE

Pb+Pb @ sqrt(s) = 2.76 ATeV

2010-11-08 11:29:42
Fill : 1444
Run : 137124
Event : 0x00000000271EC693

Charged particle multiplicity: √s dependence

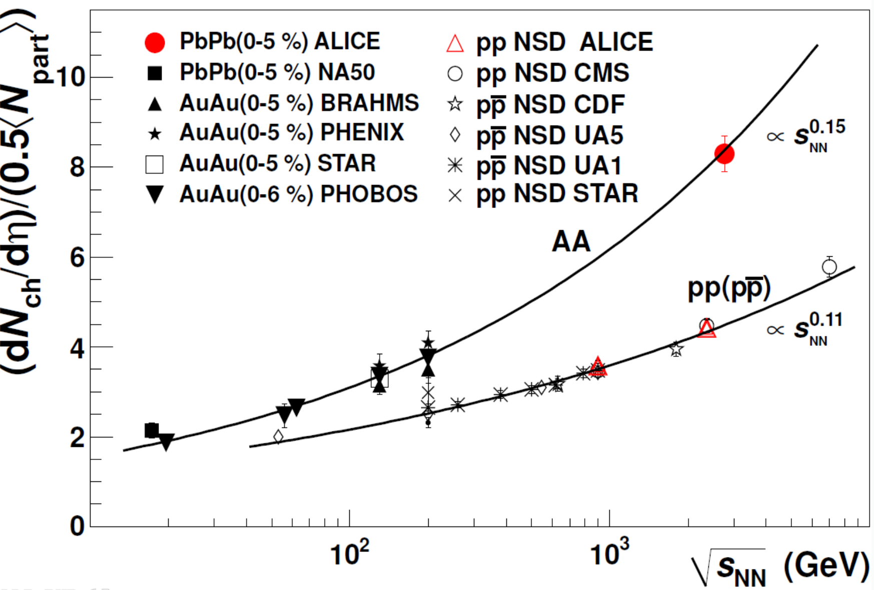

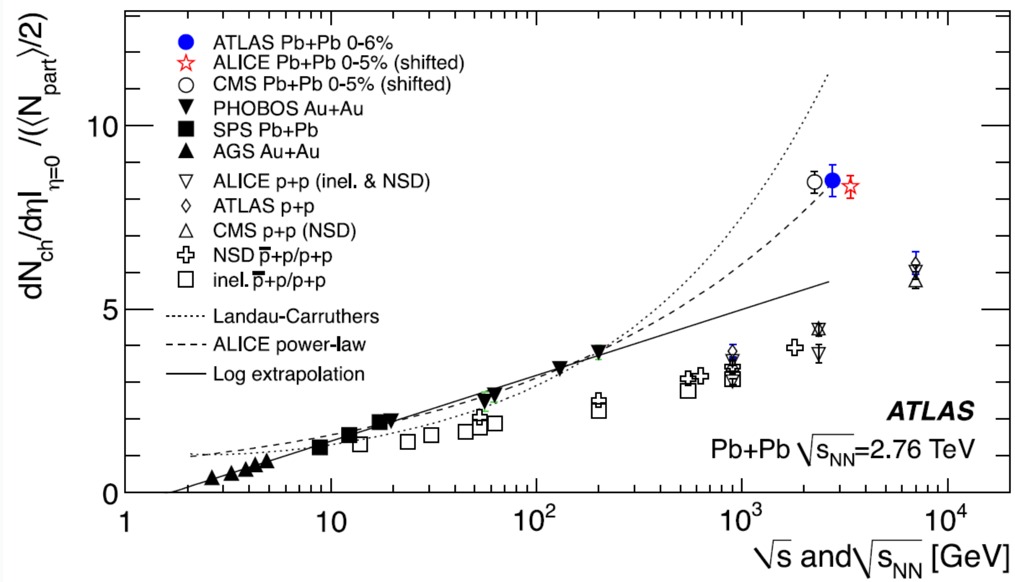

ALICE: Phys. Rev. Lett. 105 (2010) 252301, ATLAS:Phys. Lett.B 710 (2012) 363, CMS:JHEP 1108(2011) 141

- An increase by a factor 2.2, in the pseudorapidity density is observed at $\sqrt{s_{NN}}$=2.76 TeV for Pb-Pb compared to $\sqrt{s_{NN}}$=0.2 TeV for Au-Au.
- Energy dependence is steeper for heavy-ion collisions than for pp and $p\bar{p}$ collisions
- The average multiplicity per participant pair a factor 1.9 higher than that for pp and $p\bar{p}$ collisions at similar energies.

Interplay of N_{part} and N_{coll} dependence in the particle production mechanism in heavy ion collisions

$dN_{ch}/d\eta$@LHC: Model predictions/comparison

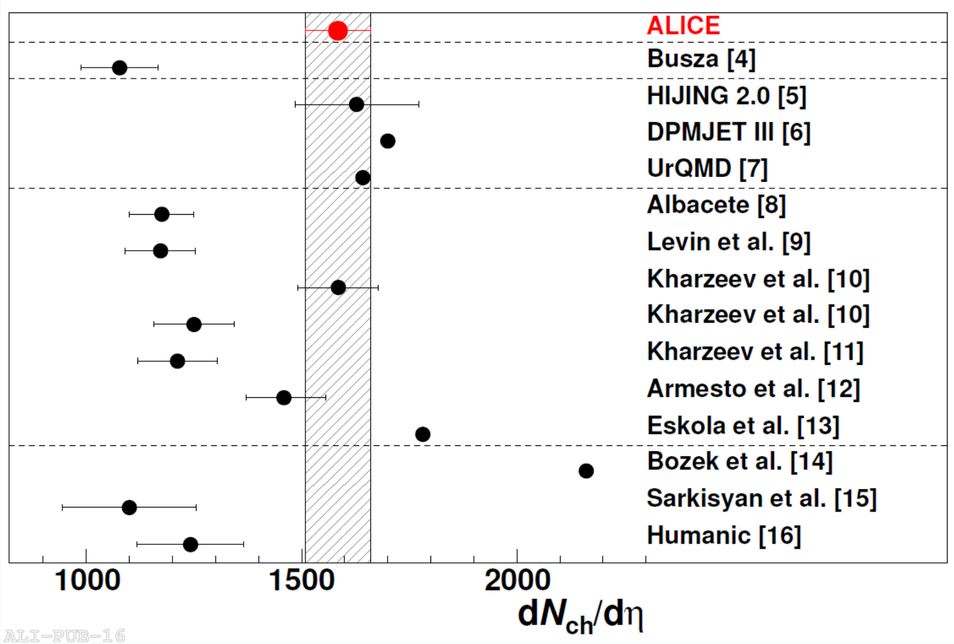

- [4]: Empirical extrapolation from lower energy data
- Perturbative-QCD-inspired Monte Carlo event generators:
  - [5] based on the HIJING model tuned to 7 TeV pp data without jet quenching
  - [6] based on the dual parton model
  - [7] based ultrarelativistic quantum molecular dynamics model

- [8-12]: Models based on initial-state gluon density saturation
- [13]: A hybrid model based on hydrodynamics and saturation of final-state phase space of scattered partons
- [14]: A hydrodynamic model in which multiplicity is scaled from p+p collisions
- [15] Model incorporating scaling based on Landau hydrodynamics
- [16] A calculation based on modified PYTHIA and hadronic rescattering

$dN_{ch}/d\eta$@LHC: Centrality dependence

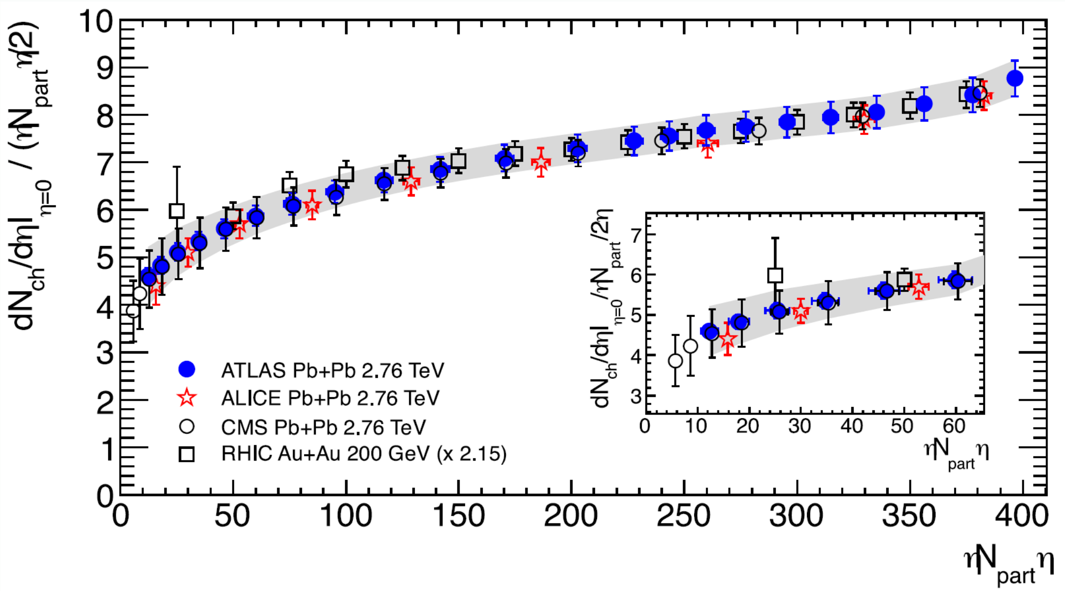

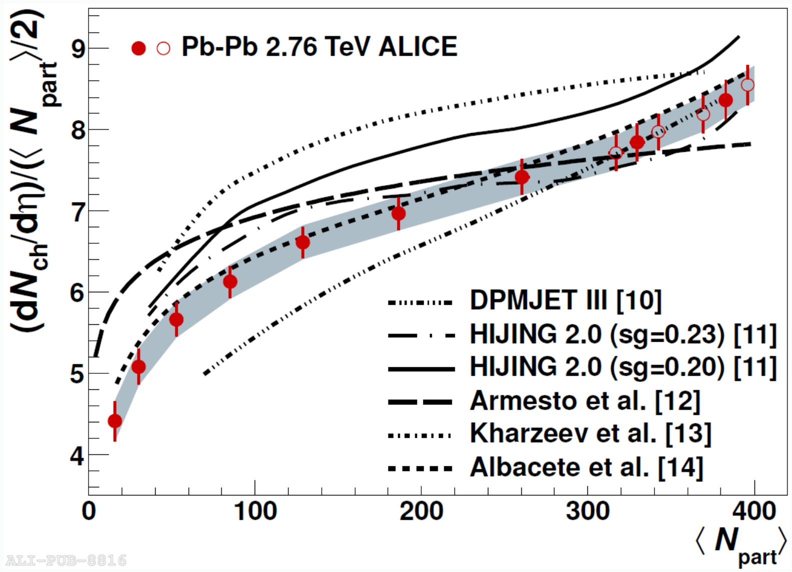

ALICE: Phys. Rev. Lett. 106 (2011) 032301, ATLAS: Phys. Lett. B 710 (2012) 363, CMS:JHEP 1108(2011) 141

Same shape of yield/participant at RHIC and LHC
The centrality dependence is well reproduced by saturation models [13,14]

Rapidity density of pions

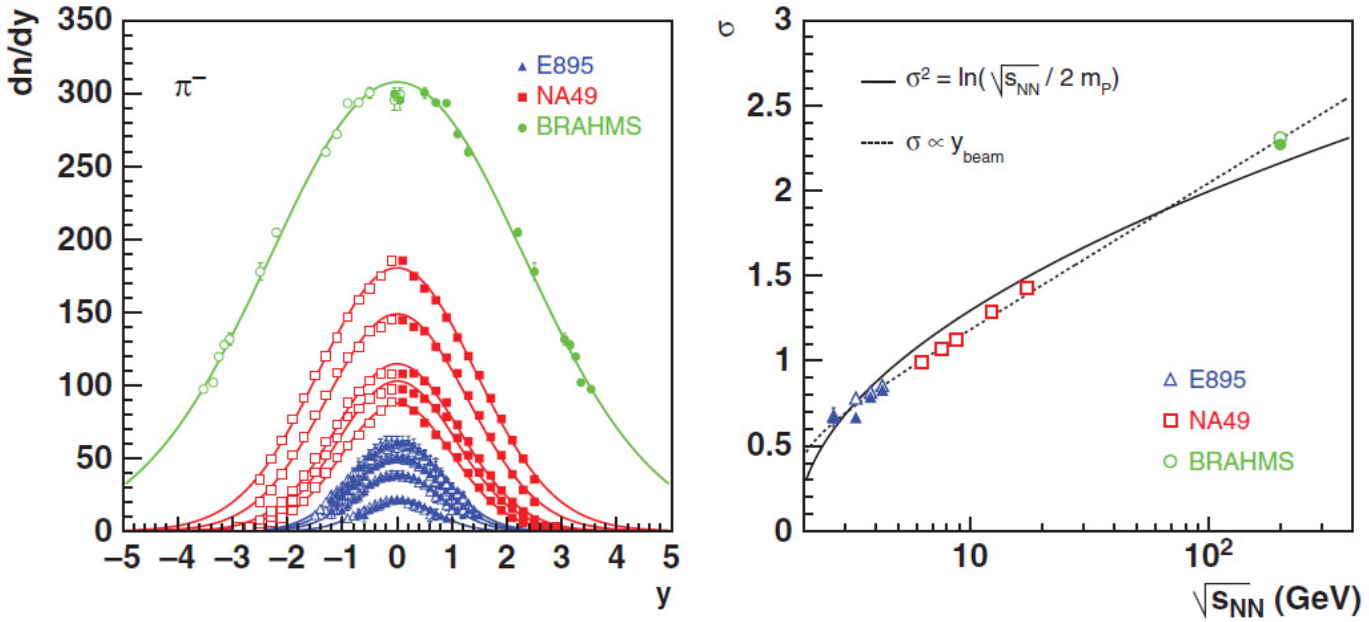

Fig. 11 *Left panel*: negative pion rapidity distributions in central Au+Au and Pb+Pb collisions from AGS via SPS to RHIC energies [61]. *Right panel*: the Gaussian rapidity width of pions vs. $\sqrt{s}$, confronted by Landau model predictions (*solid line*) [61]

C. Blume J. Phys. G31, 57(2005)

Advent of boost invariance already at $\sqrt{s_{NN}}$=200GeV

N_{ch} Pseudorapidity densities@RHIC

PHOBOS collaboration (from Miller, Reygers, Sanders, Steinberg, Ann.Rev.Nucl.Part.Sci.57 (2007) 205 [arXiv:nucl-ex/0701025

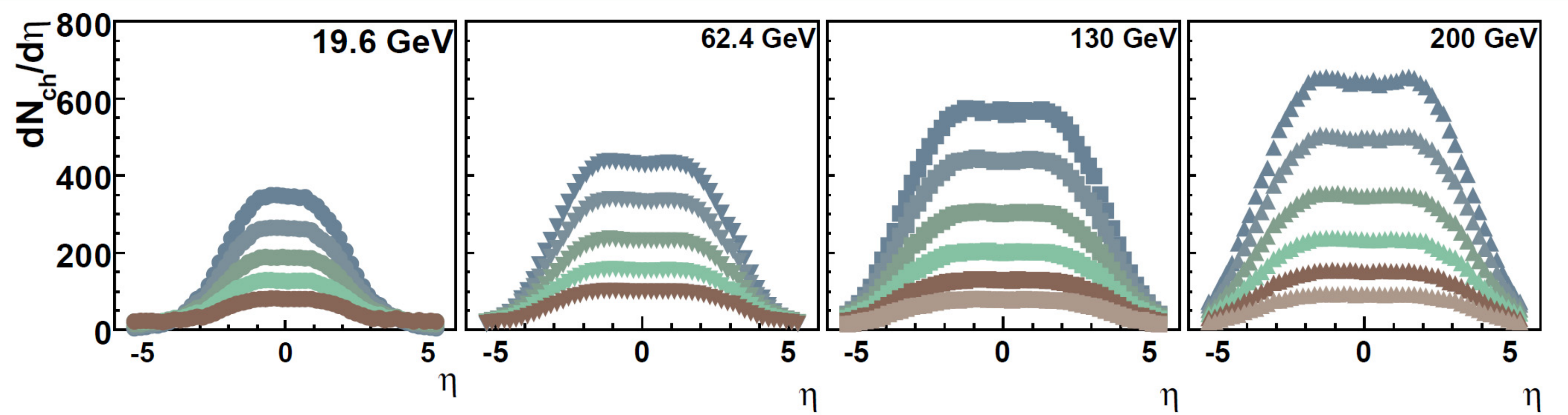

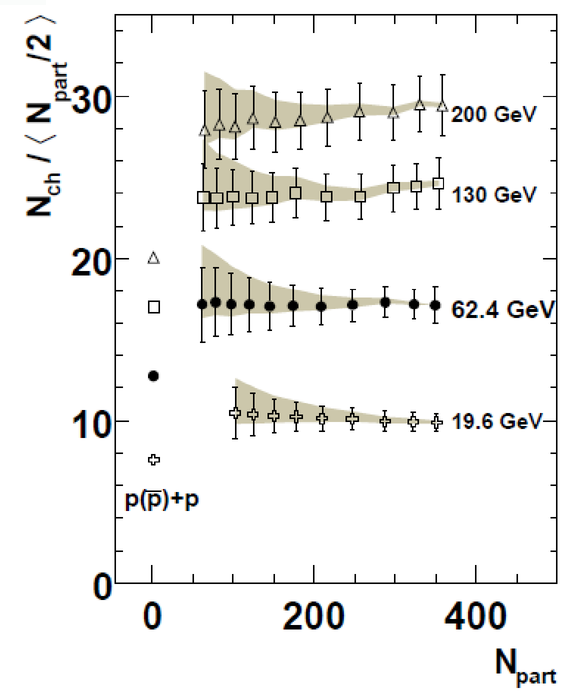

Charged particle pseudorapidity densities increase:

- with centrality (different colors) and
- with energy

Broader distributions for higher energies

Total multiplicity proportional to N_{par}

$dN_{ch}/d\eta$@LHC

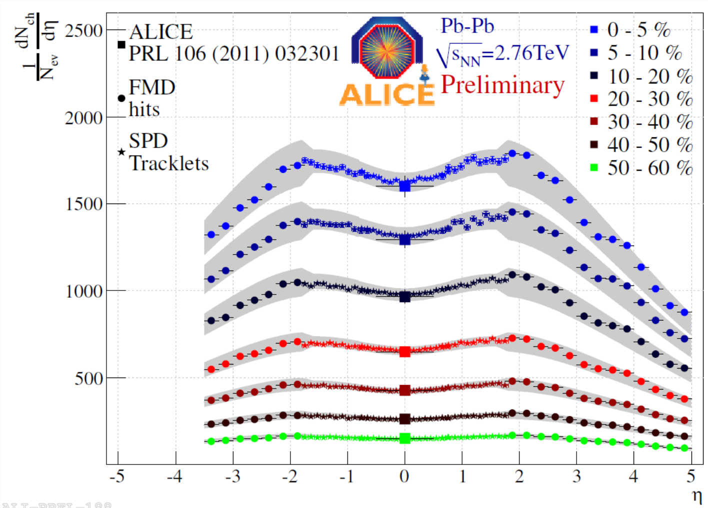

QM2011

Phys. Lett. B 710 (2012) 363

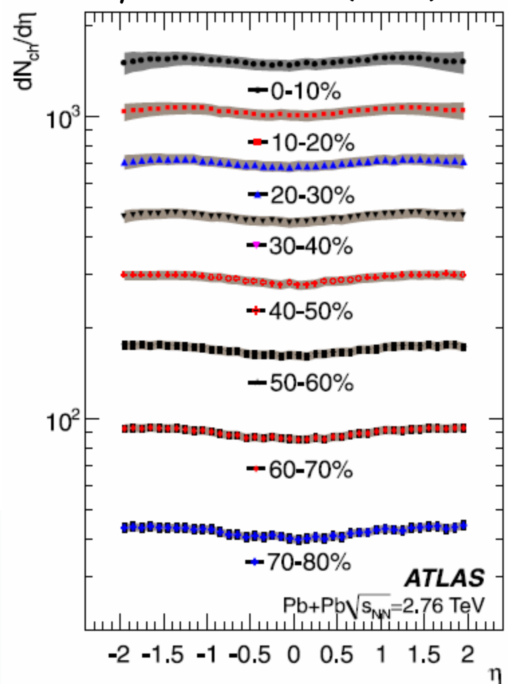

JHEP 1108(2011)141

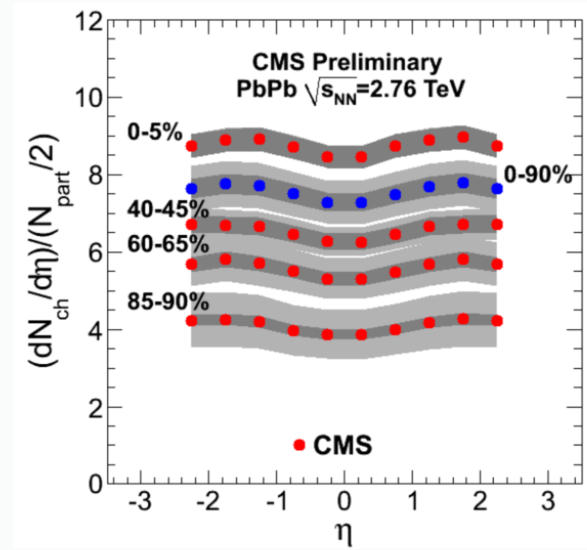

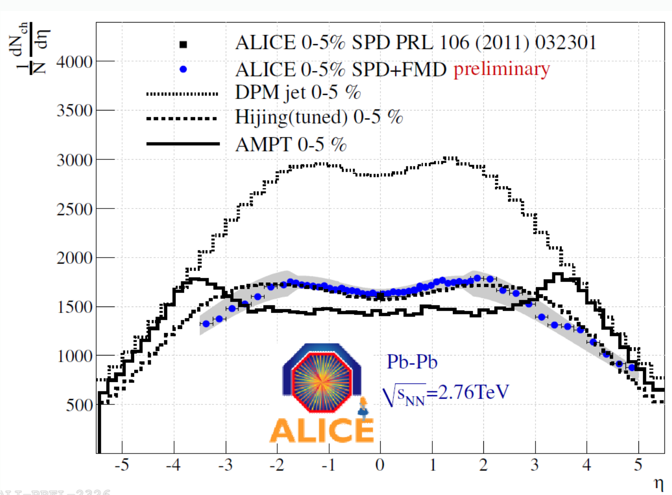

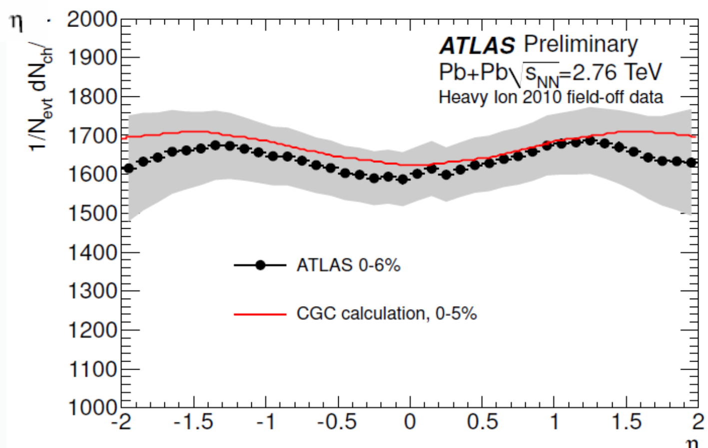

Transverse Energy

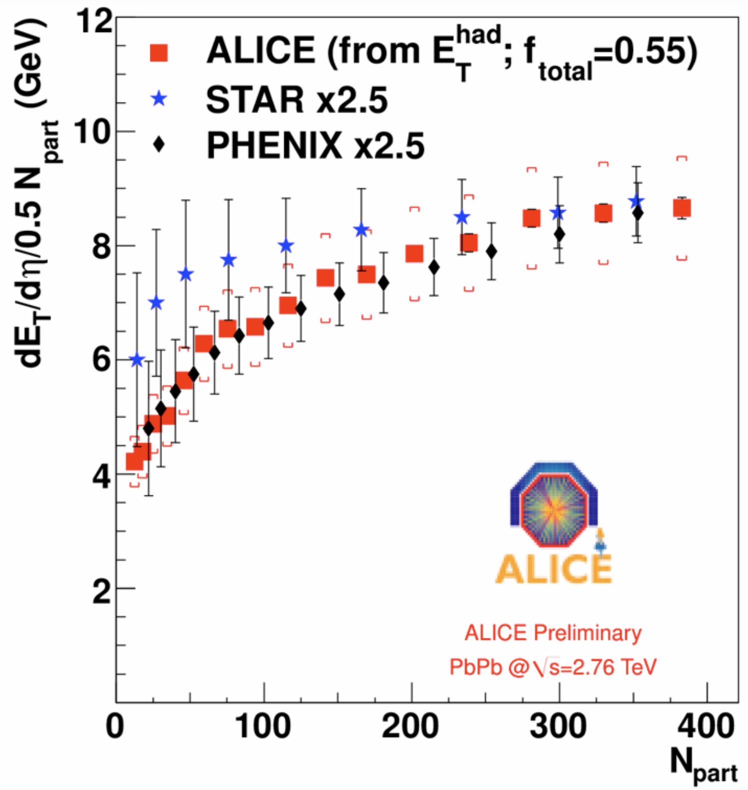

PRC70 (2004) 054907
PRC71 (2005) 034908

- E_T from charged hadrons measured by tracking detectors

$$E_T = \sum_i E_i \sin\theta_i$$

$$E_i = E_i^{tot} - m_N : baryons$$
$$E_i = E_i^{tot} + m_N : antibaryons$$
$$E_i = E_i^{tot} : others$$

- Centrality dependence similar to RHIC
- Similar dependence as $N_{ch} \rightarrow E_T/N_{ch}$ independent of centrality

$$\varepsilon_{central}^{LHC} = \frac{1}{\tau_o A}\frac{dE_t}{dy}\Big|_{y=0} \approx \frac{1}{\tau_o A}\frac{dE_t}{d\eta}, A \approx \pi R^2 = 109\, fm^2$$

$$\frac{dE_t}{d\eta} \approx 1700 GeV$$

$$\varepsilon_{central}^{LHC} \approx 16 GeV / fm^3$$

Transverse energy: √s dependence

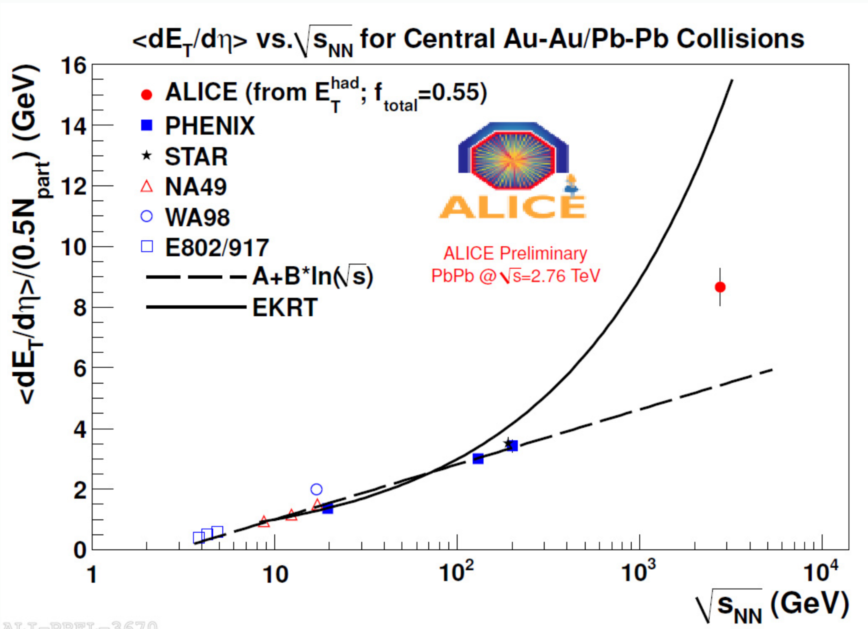

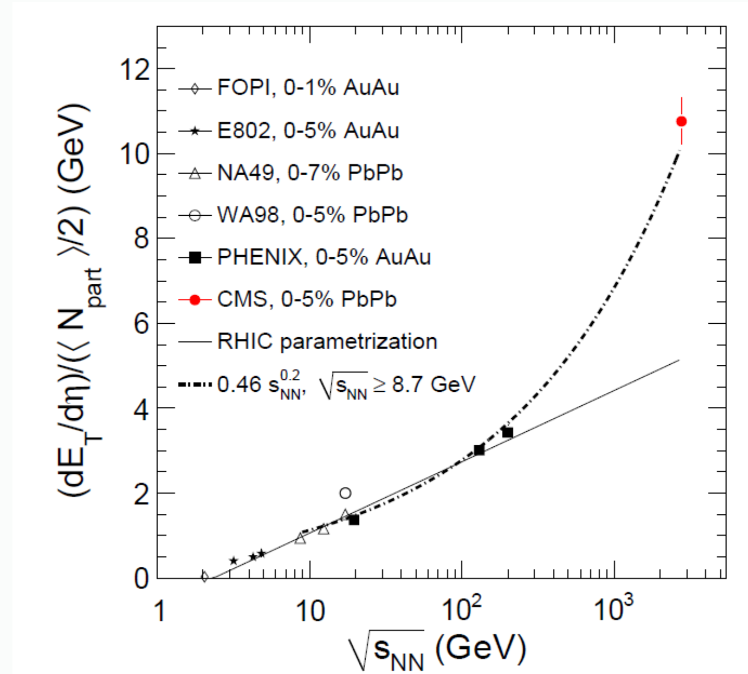

CMS: arxiv:1205.2488v1

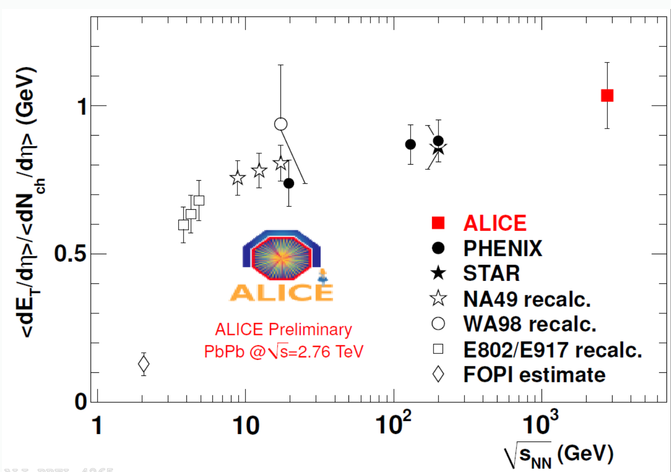

- Increase on E_T follows/consistent increase on N_{ch} , N_{part} and $\langle p_T \rangle$
- E_T/N_{ch} increases slightly with $\sqrt{s}$

Spectra

Low p_t: Integrated particle yields
High p_t: Jet quenching

Transverse momentum spectrum in pp collisions

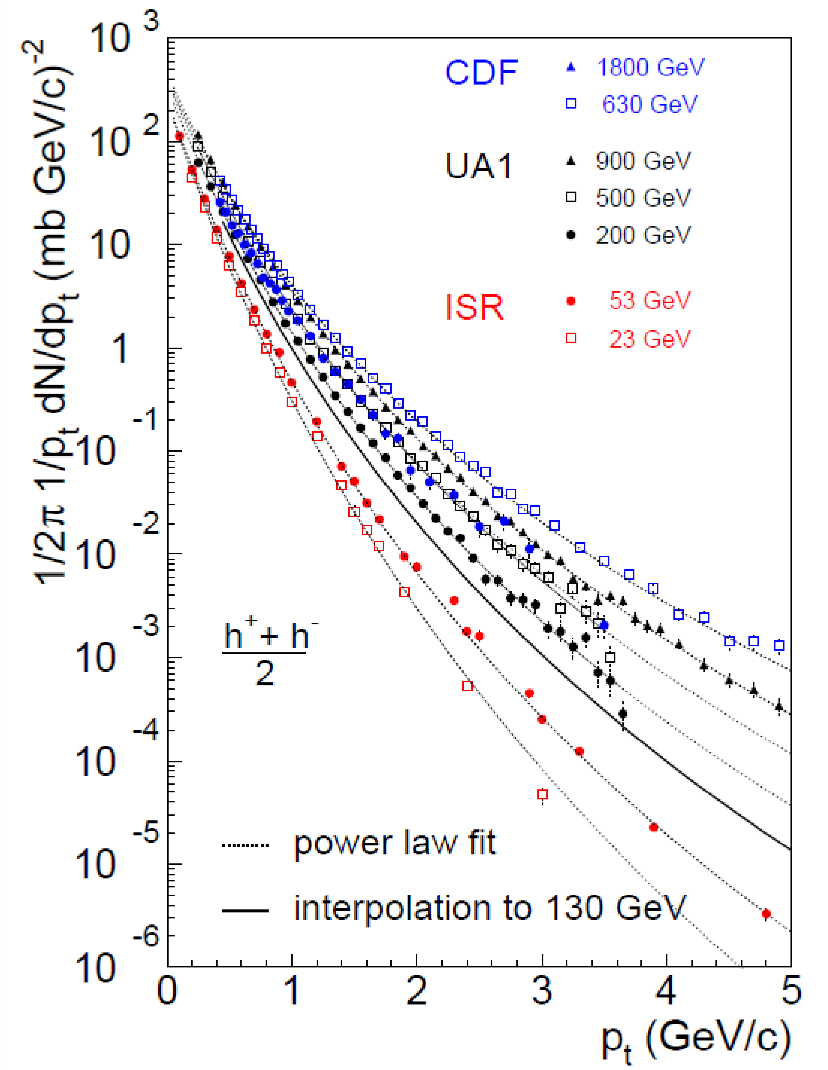

Invariant cross section:

$$E\frac{d^3\sigma}{d^3p} = \frac{d^3\sigma}{d\phi\, dy\, p_T\, dp_T} = \frac{1}{2\pi p_T}\frac{d^2\sigma}{dp_T\, dy}$$

Invariant yield:

$$\frac{1}{2\pi p_T}\frac{d^2N}{dp_T\, dy}$$

Low p_T: exponential

$$\frac{dN}{p_T\ dp_T} \propto e^{-p_T/T}$$

High p_T: power law (pQCD)

$$\frac{dN}{p_T\ dp_T} \propto \frac{1}{p_T^{n(\sqrt{s})}}$$

"Thermal" Spectra

Invariant spectrum of particles radiated by a thermal source:

$$E\frac{d^3N}{dp^3} = \frac{dN}{dy\, m_T\, dm_T\, d\phi} \propto E e^{-(E-\mu)/T}$$

where: $m_T = (m^2+p_T^2)^{\frac{1}{2}}$ transverse mass (Note: requires knowledge of mass)

$\mu = b\,\mu_b + s\,\mu_s$ grand canonical chem. potential

T temperature of source

Neglect quantum statistics (small effect) and integrating over rapidity gives:

$$\frac{dN}{m_T\, dm_T} \propto m_T\, K_1(m_T/T) \xrightarrow{m_T \gg T} \sqrt{m_T}\, e^{-m_T/T}$$

R. Hagedorn, Supplemento al Nuovo Cimento Vol. III, No.2 (1965)

At mid-rapidity $E = m_T \cosh y = m_T$ and hence: $\frac{dN}{m_T\, dm_T} \propto m_T\, e^{-m_T/T}$ "Boltzmann"

Isotropic thermal source:

$$\frac{dN}{dy} \propto \left(m^2 T + \frac{2mT^2}{\cosh y} + \frac{2T^2}{\cosh^2 y} \right) e^{-(m\cdot\cosh y/T)}$$

"Thermal" Spectra and Flow

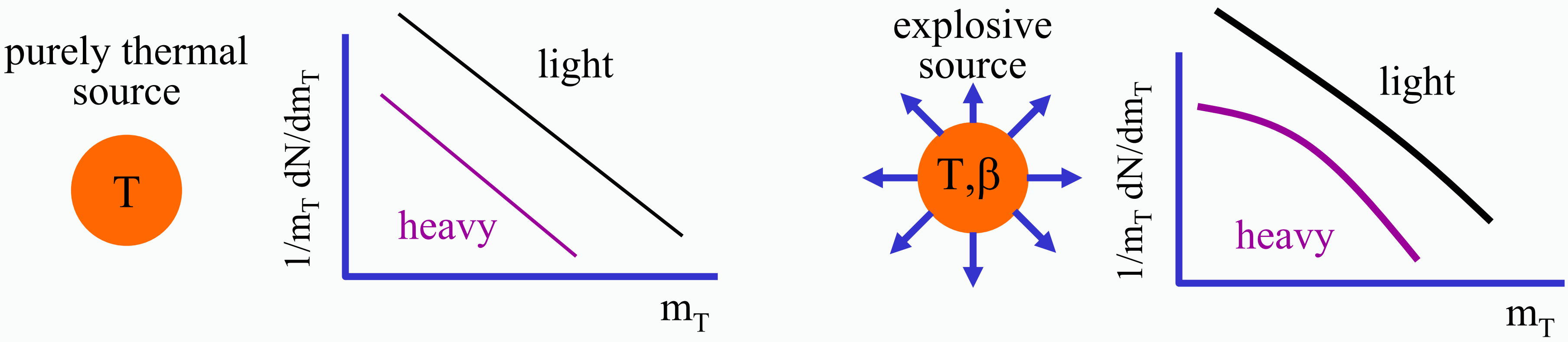

Due to collective radial flow different spectral shapes for particles of differing mass. Spectral shape is determined by at least T, β_T

$$T_{measured} = \begin{cases} T_{th} + m\langle\beta_T\rangle^2 & \text{for} \quad p_T \leq m \\ T_{th}\sqrt{\dfrac{1+\langle\beta_T\rangle}{1-\langle\beta_T\rangle}} & \text{for} \quad p_T >> m \quad \text{(blue shift)} \end{cases}$$

Blast wave model

A hydrodynamic inspired description of spectra

Schnedermann, Sollfrank, Heinz, Phys. Rev. C 48 (1993) 2462

$$\frac{dN}{m_T dm_T} \propto \int_0^R r\,dr\, m_T\, I_0\left(\frac{p_T \sinh\rho}{T}\right) K_1\left(\frac{m_T \cosh\rho}{T}\right)$$

with

transverse velocity distribution $\beta_r(r) = \beta_s \left(\frac{r}{R}\right)^n$

and boost angle (boost rapidity) $\rho = \tanh^{-1} \beta_r$

E. Schnedermann and U. Heinz, PRC50, 1675 (1994)

$$\frac{1}{m_T}\frac{dN}{dm_T} \propto m_T K_1\left(\frac{m_T \cosh\eta_T}{T_{kin}}\right) I_0\left(\frac{p_T \sinh\eta_T}{T_{kin}}\right)$$

$$\eta_T = \tanh^{-1} \beta_T$$

F. Retiere and M. Lisa PRC70; PHENIX PRL88

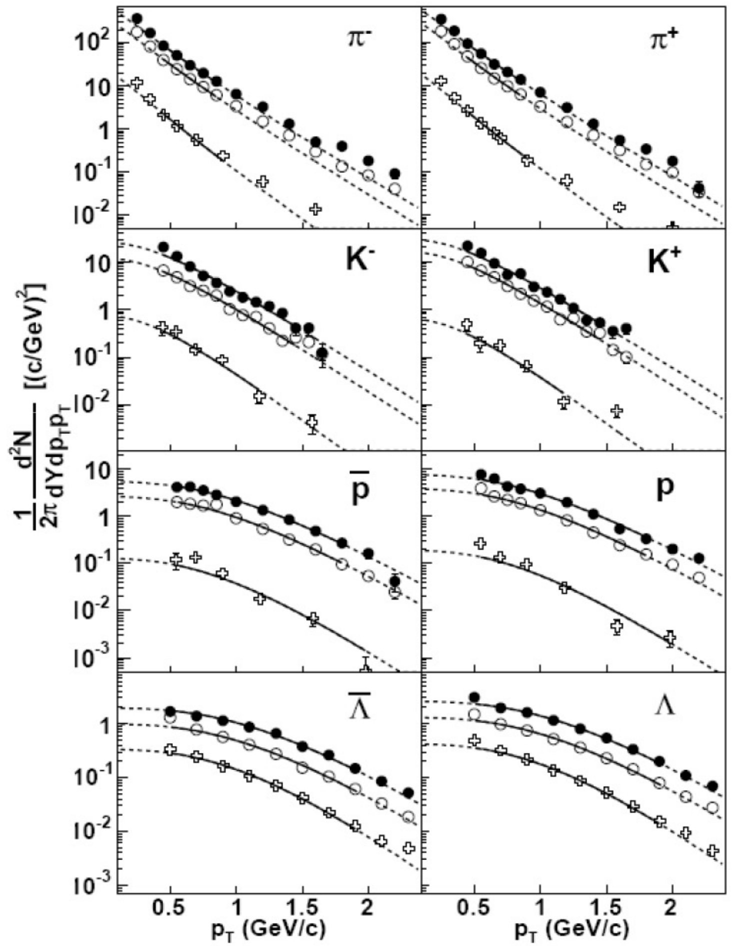

FIG. 49: Comparison of the data with the blast-wave calculations performed with the best fit parameters in three centrality bins. The closed circles are central data, the open circles are mid-central data and the crosses are peripheral data. The plain lines show the blast wave calculation within the fit range while the dash lines show the extrapolation over the whole range.

Transverse Flow excitation function

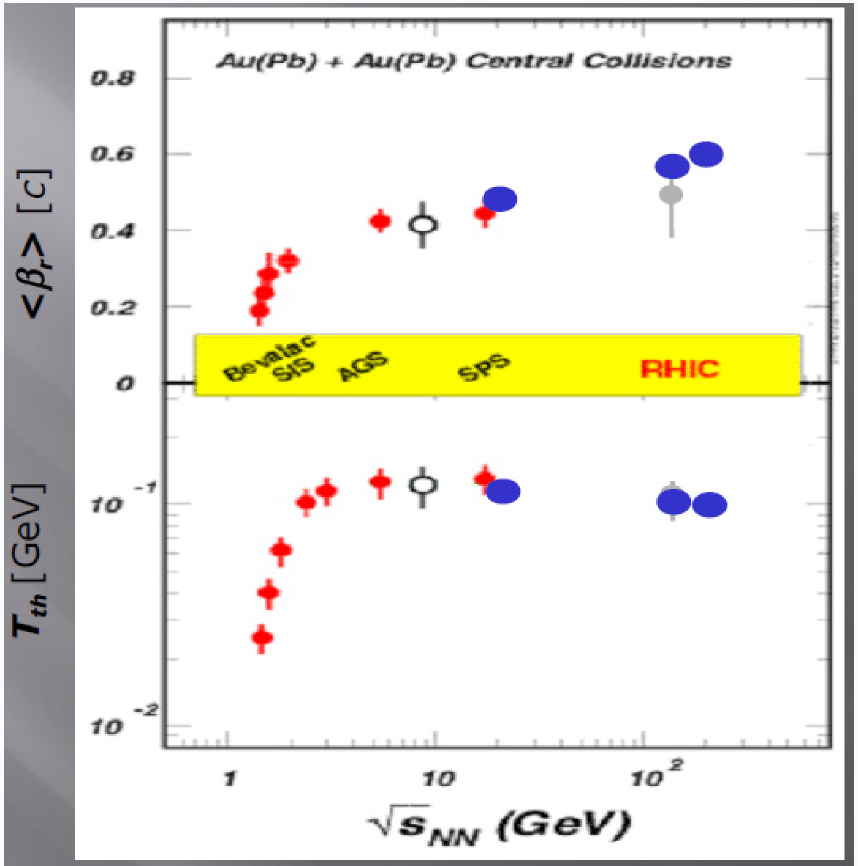

Xu N and Kaneta M 2002 *Nucl. Phys. A* 698 306

Saturation or slow increase from SPS to RHIC

Identified particle spectra@PbPb (LHC-RHIC)

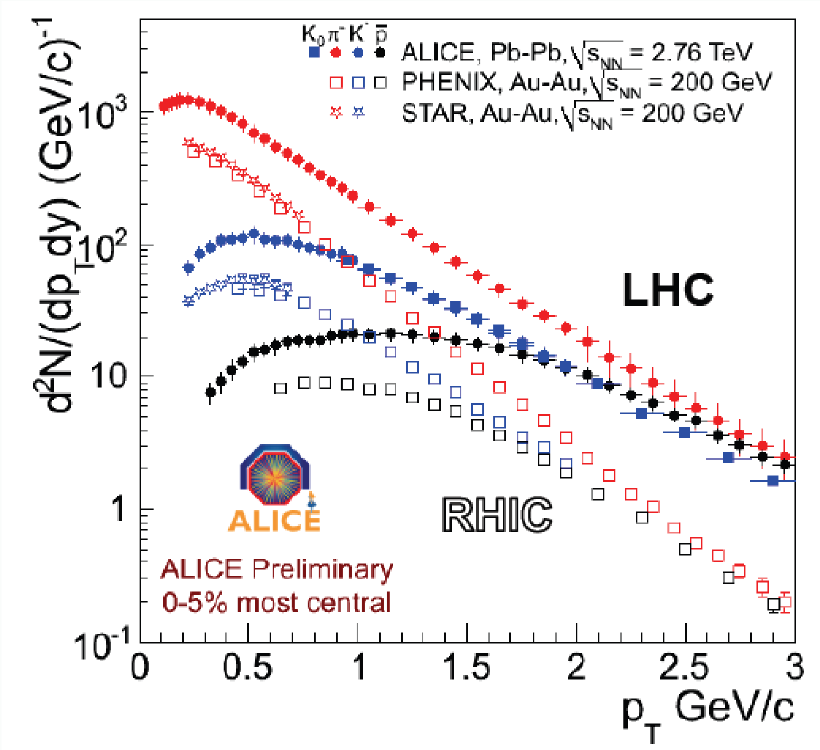

Significant change in slope compared to RHIC; largest for protons

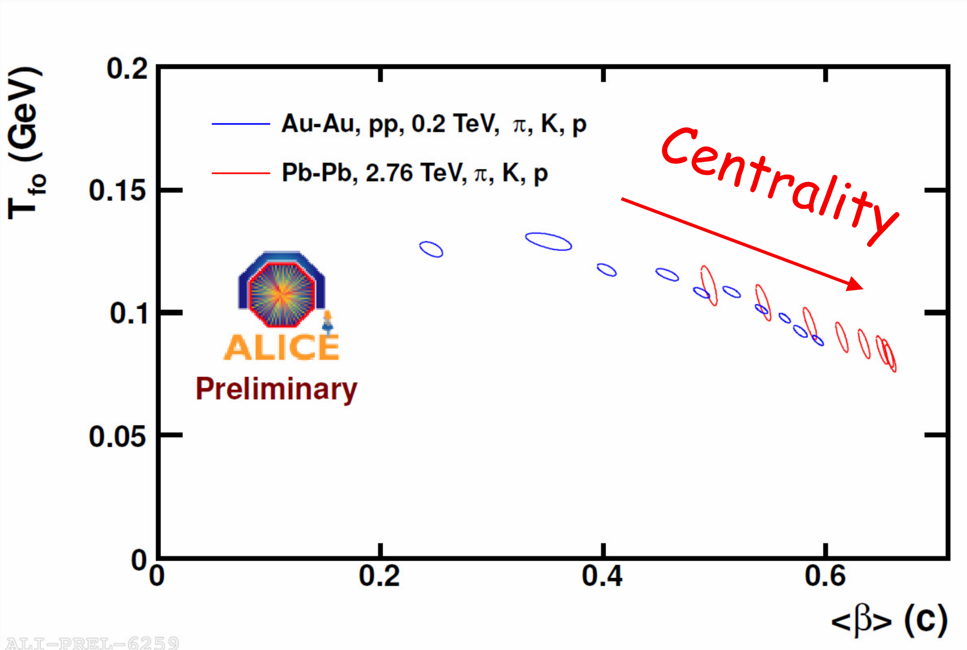

Very strong radial flow, β~0.66
Stronger than predicted by most recent hydro

Identified particle spectra@PbPb (LHC)

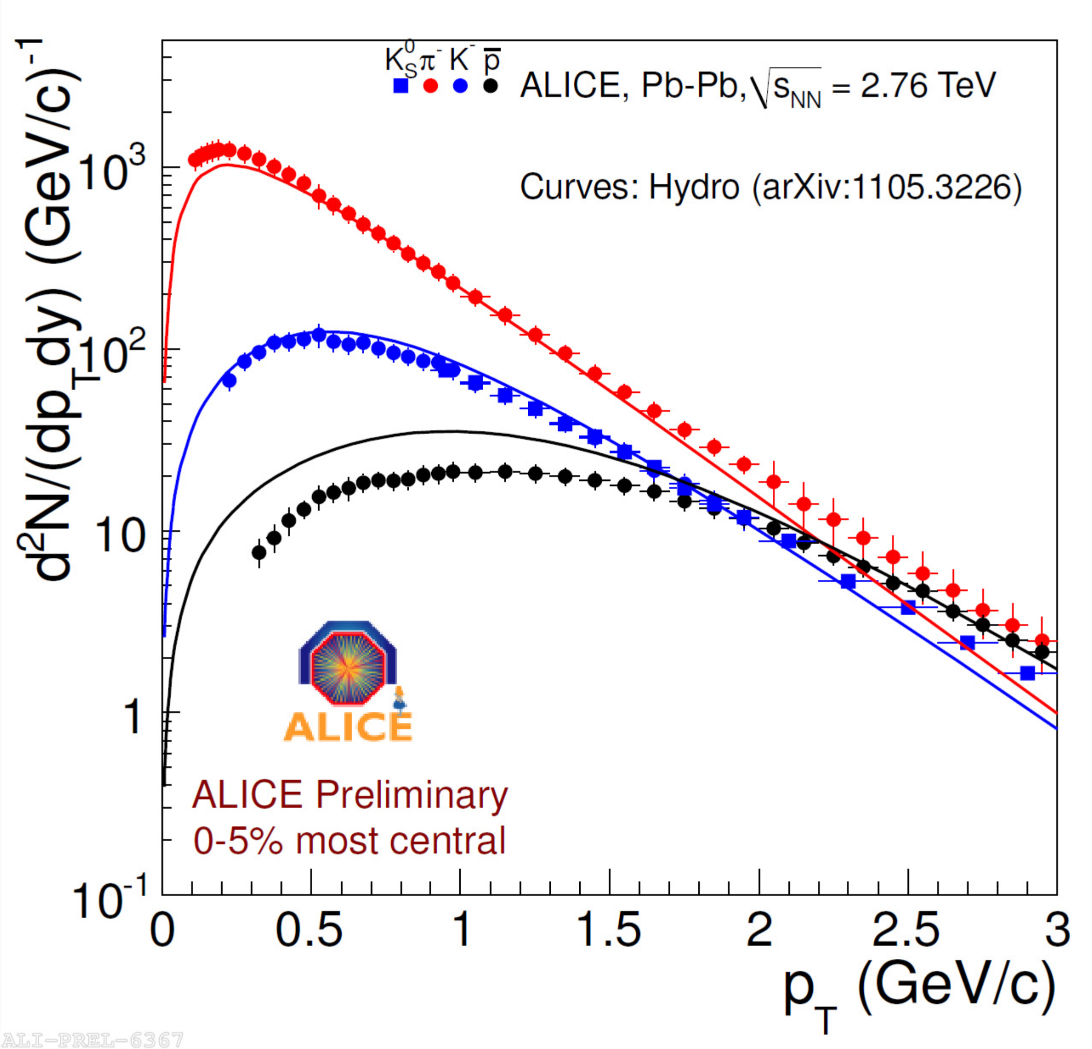

Hydro predictions quite good for pions and Kaons. Some discrepancies for protons

C. Shen, U. Heinz, P. Huovinen, and H. Song Hydro: arXix:1105.3226

Thermal Model and particle abundancies

- Assume chemically equilibrated system at freeze-out (constant T_{ch} and μ)
- Composed of non-interacting hadrons and resonances
- Given T_{ch} and μ 's, particle abundances (n_i's) can be calculated in a grand canonical ensemble

Partition function:

$$\ln Z_i = \frac{Vg_i}{2\pi^2}\int_o^\infty \pm p^2 dp \ln(1 \pm \exp(-(E_i - \mu_i)/T))$$

Particle densities:

$$n_i = \frac{g}{2\pi^2}\int_0^\infty \frac{p^2 dp}{e^{(E_i(p)-\mu_i)/T} \pm 1}, \quad E_i = \sqrt{p^2 + m_i^2}$$

- Obey conservation laws: Baryon Number, Strangeness, Isospin

$$\mu = \mu_B B_i + \mu_S S_i + \mu_{I3} I_i^3, \qquad V\sum_i n_i B_i = Z + N, \qquad V\sum_i n_i S_i = 0, \qquad V\sum_i n_i I_i^3 = \frac{Z - N}{2}$$

- Short-lived particles and resonances need to be taken into account

Measure particle ratios → Extract T_{ch} and μ → Calculate particle ratios
Compare particle abundancies
Predict

The hadronic mass spectrum

Phys. Lett. B673 (2009) 142

- Complete mass states published in PDG 2008, Phys. Lett. B 667 (2008) 1.
- σ meson included [f_0(600)]:
  - m_σ = 484 ± 17 MeV, Γ_σ = 510 ± 20 MeV
  - García-Martín, Pelaez, Yndurain, Phys. Rev. D 76 (2007) 074034

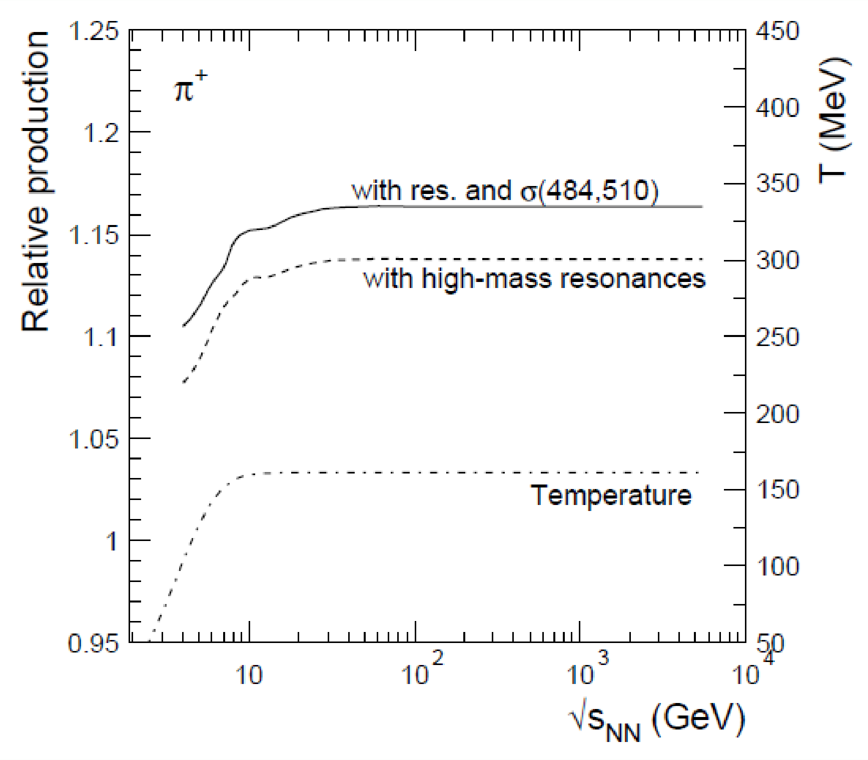

Increase on pion yield

The thermal fits

Phys. Lett. B673 (2009) 142

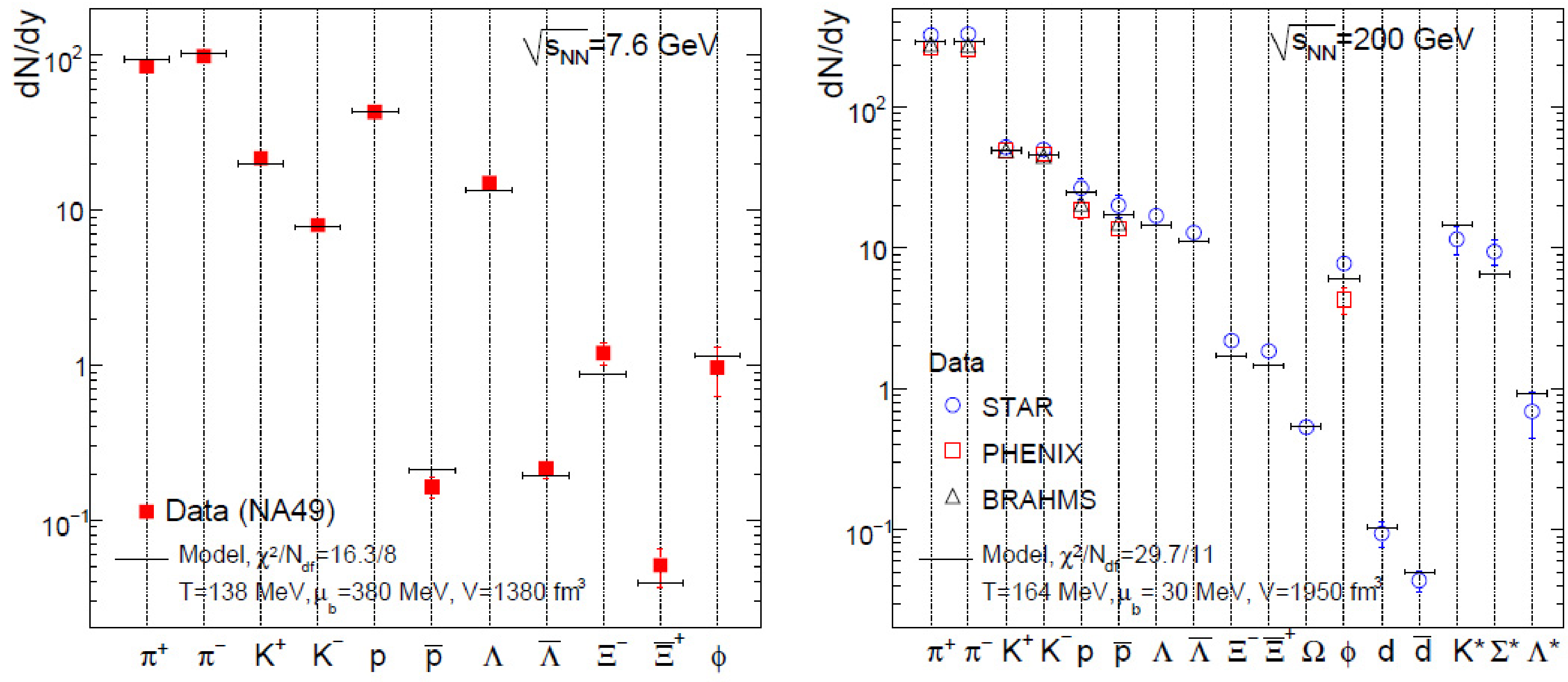

Figure 2. Experimental hadron yields and model calculations for the parameters of the best fit at the energies of 7.6 (left panel) and 200 GeV (right panel; the Ω yield includes both Ω^- and $\bar{\Omega}^+$).

Good agreement between experimental yields and thermal model

Energy dependence of T and μ. Comparison of different models

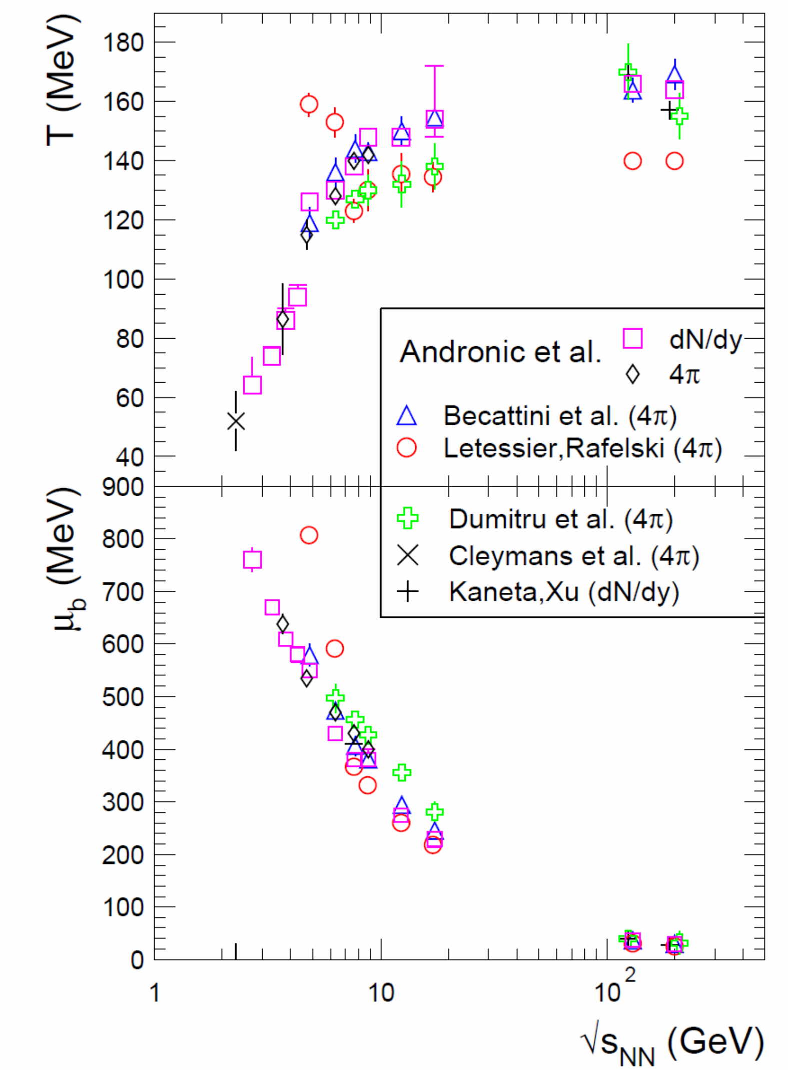

Nucl. Phys.A834(2010)237c

- Becattini et al.: γ_S
  - Phys. Rev. C 73 (2006) 044905
  - Phys. Rev. C 78 (2008) 054901
- Rafelski et al.: $\gamma_{S,q}$, $\lambda_{q,S,I3}$
  - Eur. Phys. J A35 (2008) 221
  - γ_S = 0.18,0.36,1.72,1.64,...
  - γ_q = 0.33,0.48,1.74.1.49,1.39,1.47,...
- Dumitru et al.: inhomogeneous freeze-out $\delta T, \delta\mu_B$
  - Phys. Rev. C 73 (2006) 024902
- Kaneta,Xu
  - nucl-th/0405608
- Cleymans et al.,
  - Phys. Rev. C 57 (1998) 3319

- THERMUS, Publicly available
  S. Wheaton , J. Cleymans, M. Hauer .
  Comp. Phys. Com. 180 (2009) 84–106

Energy dependence of T and μ

Phys. Lett. B673 (2009) 142

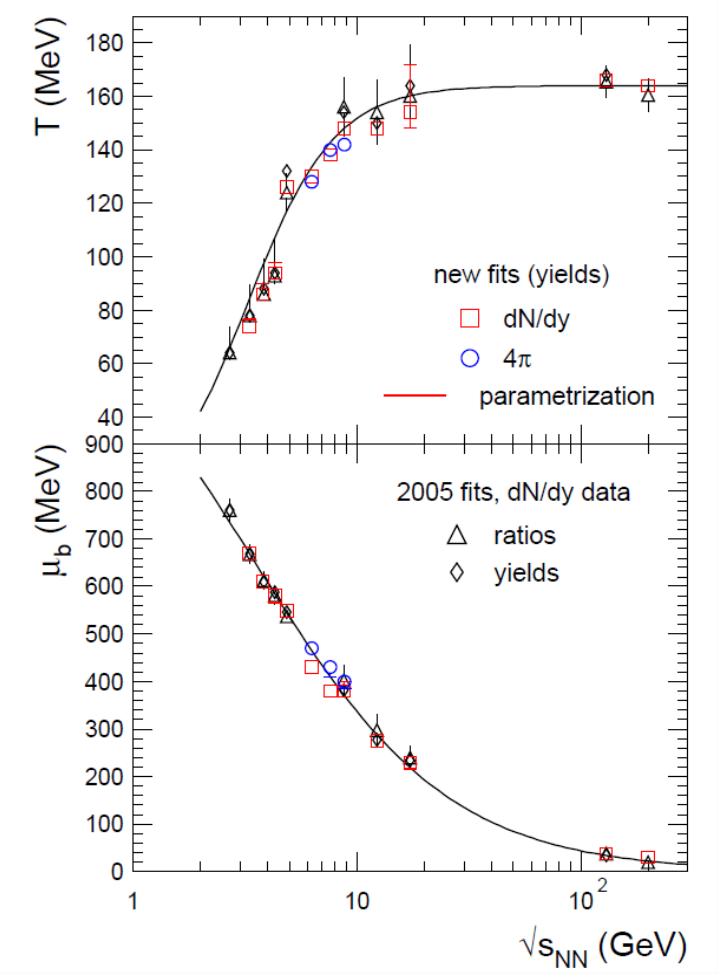

Thermal fits exhibit a limiting temperature:

T_{lim} = 164 ± 4 MeV

$$T = T_{lim}\frac{1}{1+\exp(2.60-\ln(\sqrt{s_{NN}}(\mathrm{GeV}))/0.45)}$$

$$\mu_b[\mathrm{MeV}] = \frac{1303}{1+0.286\sqrt{s_{NN}}(\mathrm{GeV})}$$

Predictions for LHC

J. Phys. G38 (2011) 124081

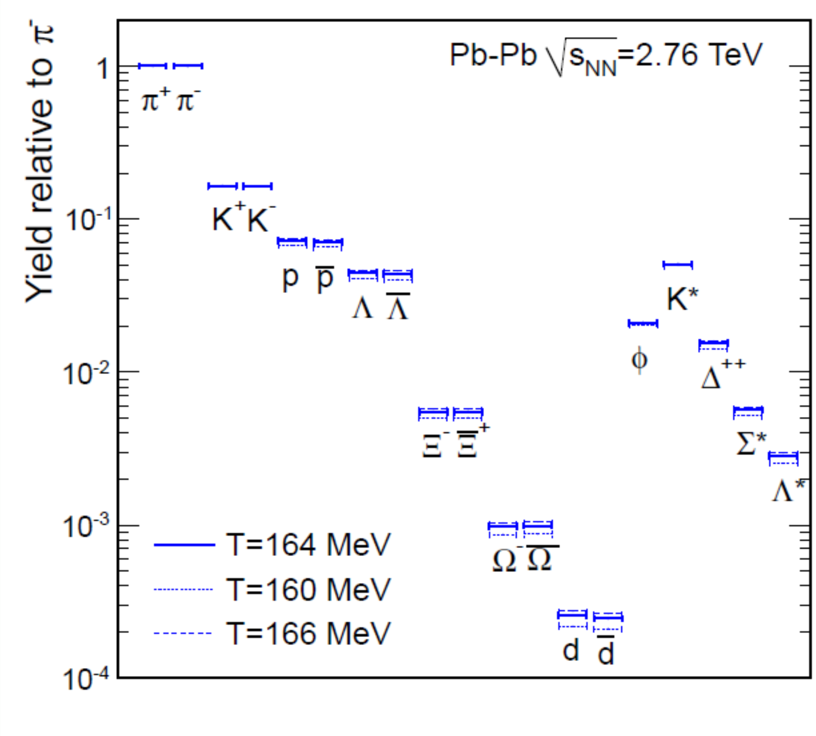

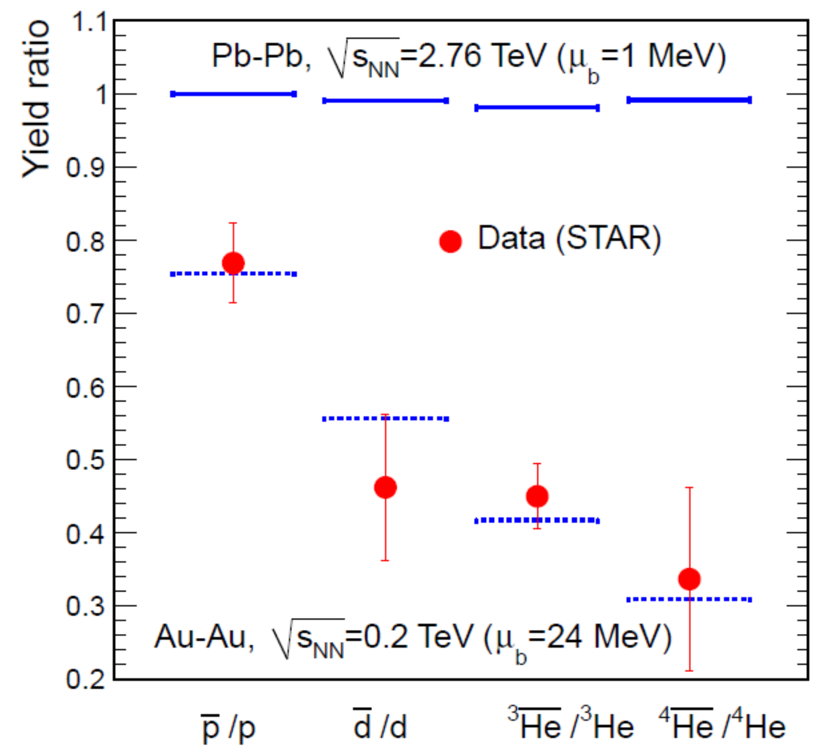

•Predictions for the production of various hadrons relative to pions. To be tested.

•Balance between matter and anti-matter production is changing considerably from RHIC to LHC energies

Phase diagram of strongly interacting matter

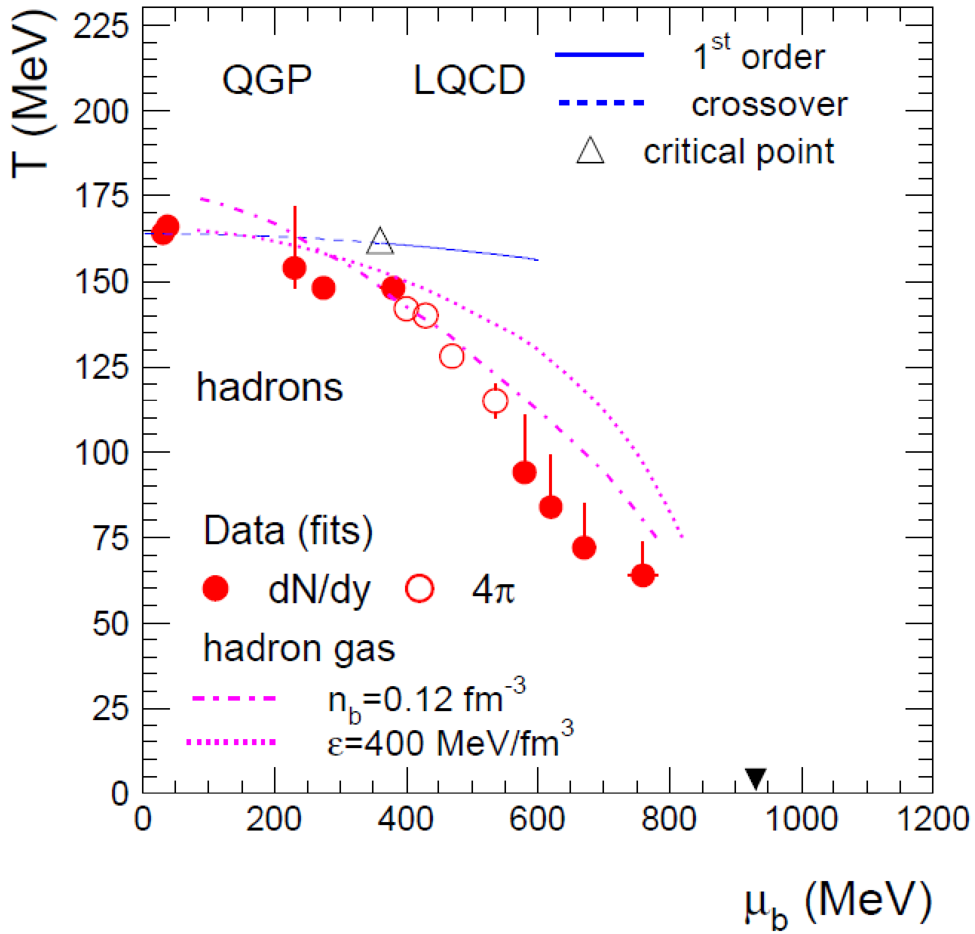

Figure 3. The phase diagram of strongly interacting matter. The points represent the results of the thermal fits. For the SPS beam energy of 40 AGeV ($\mu_b \simeq$400 MeV) we show both midrapidity (dN/dy) and full phase space (4π) fit results. The phase boundary and critical point from lattice QCD (LQCD) calculations [20] is shown together with freeze-out curves for a hadron gas at constant baryon density (baryons and anti-baryons) and energy density. The full triangle indicates the location of ground state nuclear matter (atomic nuclei).

HBT-interferometry

(Hanbury-Brown-Twiss)

The range of correlation in momentum space allows extraction of spatio-temporal extension in configuration space:

It is important to constrain models which connect to lifetime or source size

HBT

- In the 1950's by Robert Hanbury-Brown and Richard Q. Twiss:

As a means to measuring stellar radii through the angle subtended by nearby stars, as seen from the Earth's.

Phil. Mag. 45, 663(1954), Nature 177, 26 (1956), Nature 178, 1447 (1956).

2-photon correlation function: $$C = \frac{\langle I_1(t) I_2(t) \rangle}{\langle I_1(t) \rangle \langle I_2(t) \rangle}$$

Narrabri Interferometer, Australia

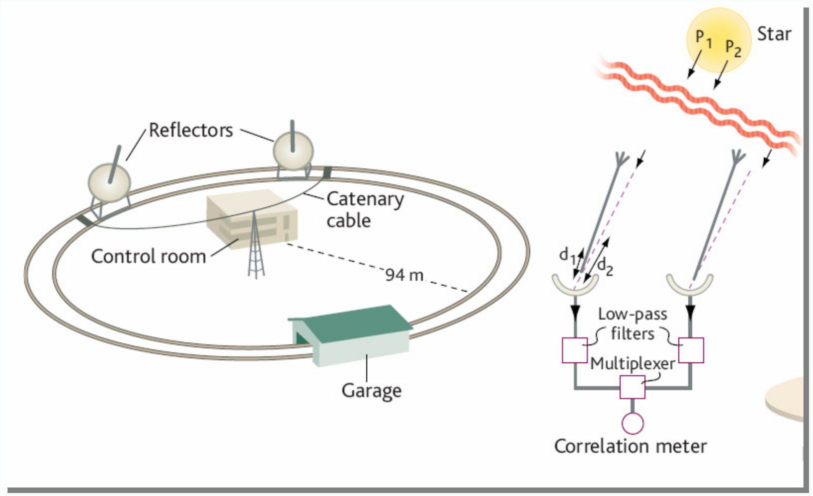

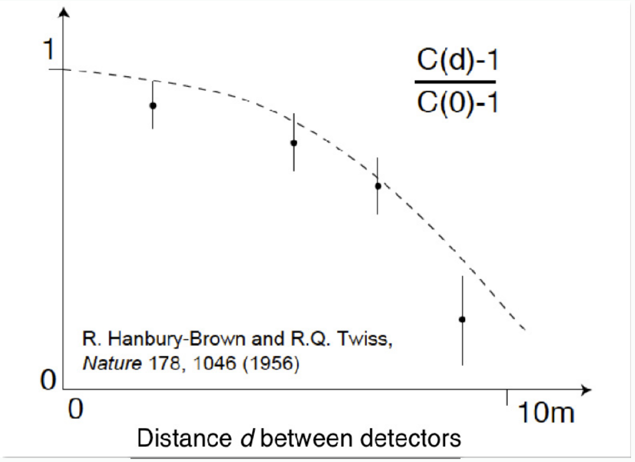

Enhancement due to Bose-Einstein statistics of photons

HBT in particle physics: GGLP

$\bar{p}p$ collisions, at 1.05 GeV/c. G. Goldhaber, S. Goldhaber, W.Y. Lee, A. Pais, Phys. Rev. 120 (1960) 300

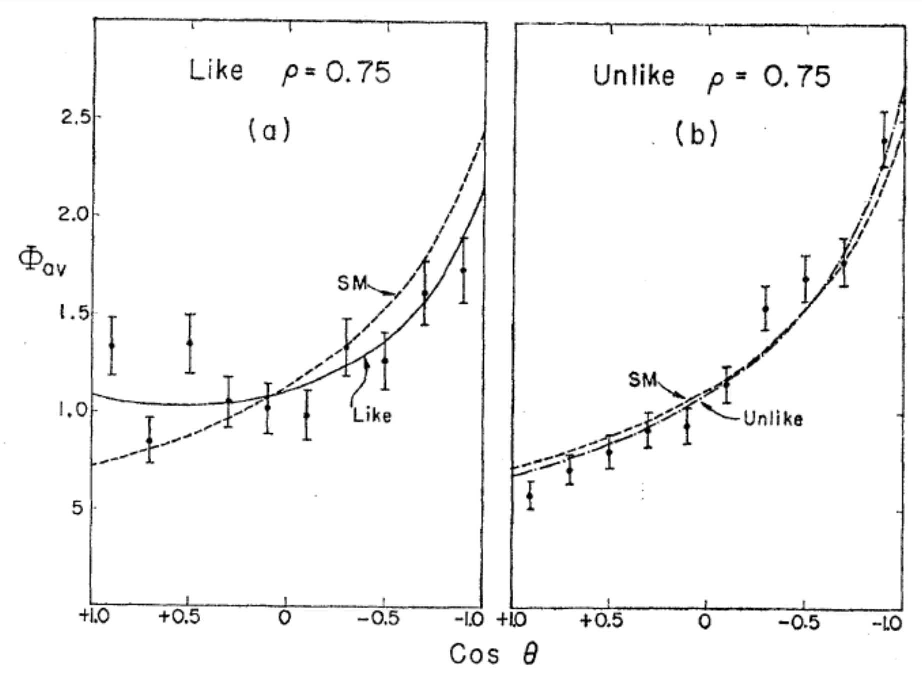

First observation in particle physics

$$p + \bar{p} \rightarrow \pi^{+} + \pi^{-}$$

HBT

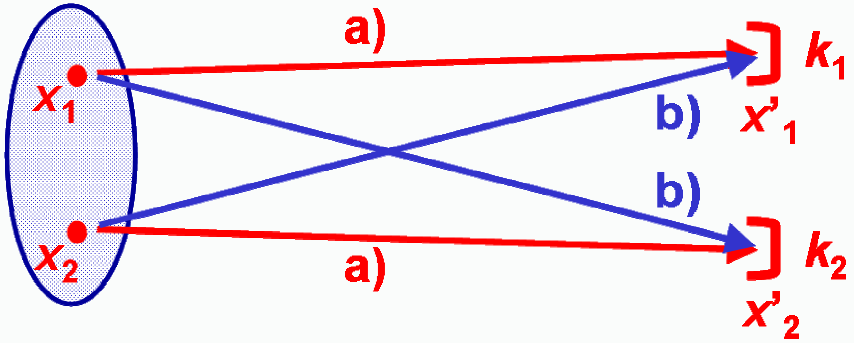

Relative momentum $q = k_1 - k_2$

Effective emission distribution: $\rho_{eff}(x, k_1, k_2) = \dfrac{\rho(x)A(k_1, x)A(k_2, x)}{\sqrt{P(k_1)P(k_2)}}$

$$\begin{aligned} P(k_1, k_2) &= P(k_1)P(k_2)\left(1 + \left|\int dx\, e^{iqx}\rho_{eff}(x, k_1, k_2)\right|^2\right) \\ &= P(k_1)P(k_2)\left(1 + |\tilde{\rho}_{eff}(q, k_1, k_2)|^2\right) \end{aligned}$$

Fourier transformed distribution

Correlation function:

$$\begin{aligned} C_2(q, k_1, k_2) &= \frac{P(k_1, k_2)}{P(k_1)P(k_2)} \\ &= 1 + |\tilde{\rho}_{eff}(q, k_1, k_2)|^2 \end{aligned}$$

Gaussian static source:

$$\rho_{eff}(r) = \frac{1}{4\pi^2 R}\exp\left(\frac{r^2}{2R^2}\right)$$

$$C_2(q) = 1 + \exp(-R^2 q^2)$$

Dynamical Sources

Particle sources expand

Differently in longitudinal and transverse direction

$\Rightarrow$ 3-dimensional radius parameters
Yano-Koonin-Podgoretskii (YKP)
Bertsch-Pratt (BP)

Interpretation of radius parameter as source size meaningless

$\Rightarrow$ Lengths of homogeneity

Radius parameter depend on transverse momentum (k_t) of the pairs

Flow introduces space momentum correlations
Also: resonance decays, jets, ...

$$k_t = \frac{1}{2} \left| \vec{p}_{t,1} + \vec{p}_{t,2} \right|$$

Bertsch-Pratt Parametrization

3-dimensional parametrization:

$$C_2(q) = 1 + \lambda\ \exp(-q_{side}^2 R_{side}^2 - q_{out}^2 R_{out}^2 - q_{long}^2 R_{long}^2 - q_{out} q_{long} R_{out-long}^2)$$

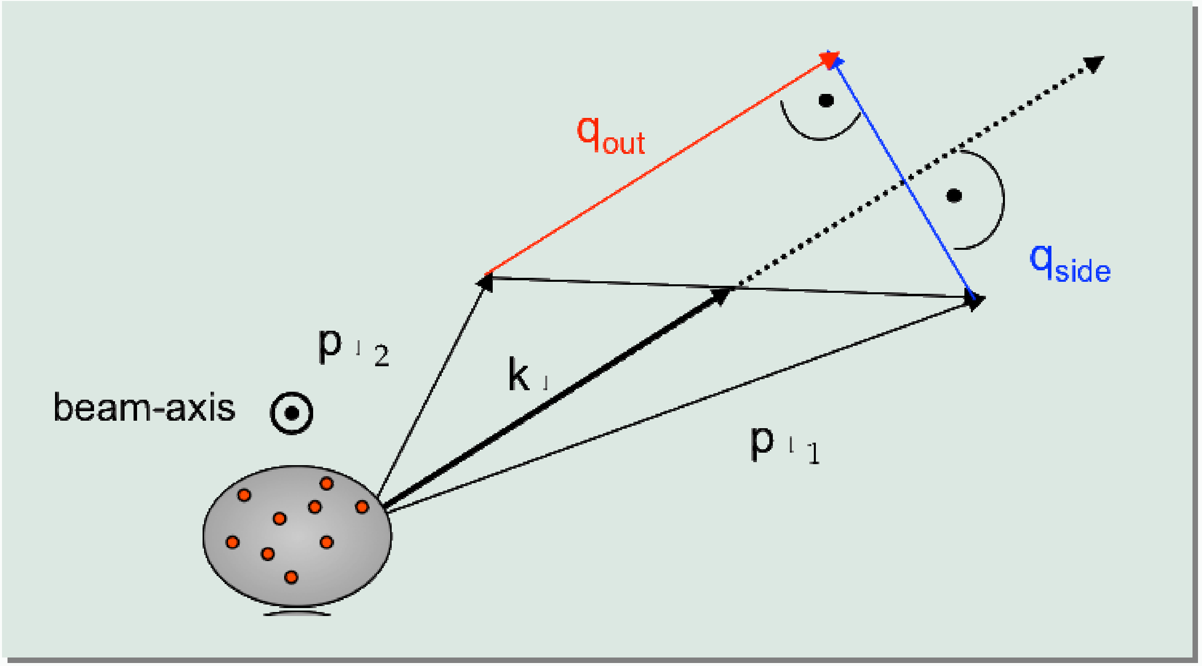

Long: defined by beam-axis

Mixed term vanishes at mid-rapidity

Radius Parameters for an Expanding Source

R_{long}: Proportional to thermal „Freeze-Out"-time τ_f
(Y. Sinyukov).

T_f: freeze-out temperature

m_T: transverse mass of the pair $m_T = \sqrt{k_t^2 + m_0^2}$

$$R_{long}^2 \approx \tau_f^2 \frac{T_f}{m_T}$$

R_{side}: Sensitive to transverse expansions-velocity β_T
(U. Heinz, B. Tomasik, U. Wiedemann)

R_{Geo}: Geometrical, static radius

$\eta_T = \tanh^{-1}(\beta_T)$

$$R_{side}^2 \approx R_{Geo}^2 \left\{1 + \frac{m_T}{T_f}\eta_T^2\right\}^{-1}$$

R_{out}: Sensitive to emission duration $\Delta\tau$

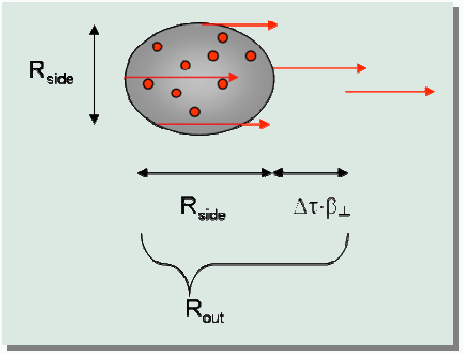

$$\Delta\tau^2 \approx \frac{1}{\beta_T^2}\left(R_{out}^2 - R_{side}^2\right)$$

Correlation function. R_{out},R_{side},R_{long}

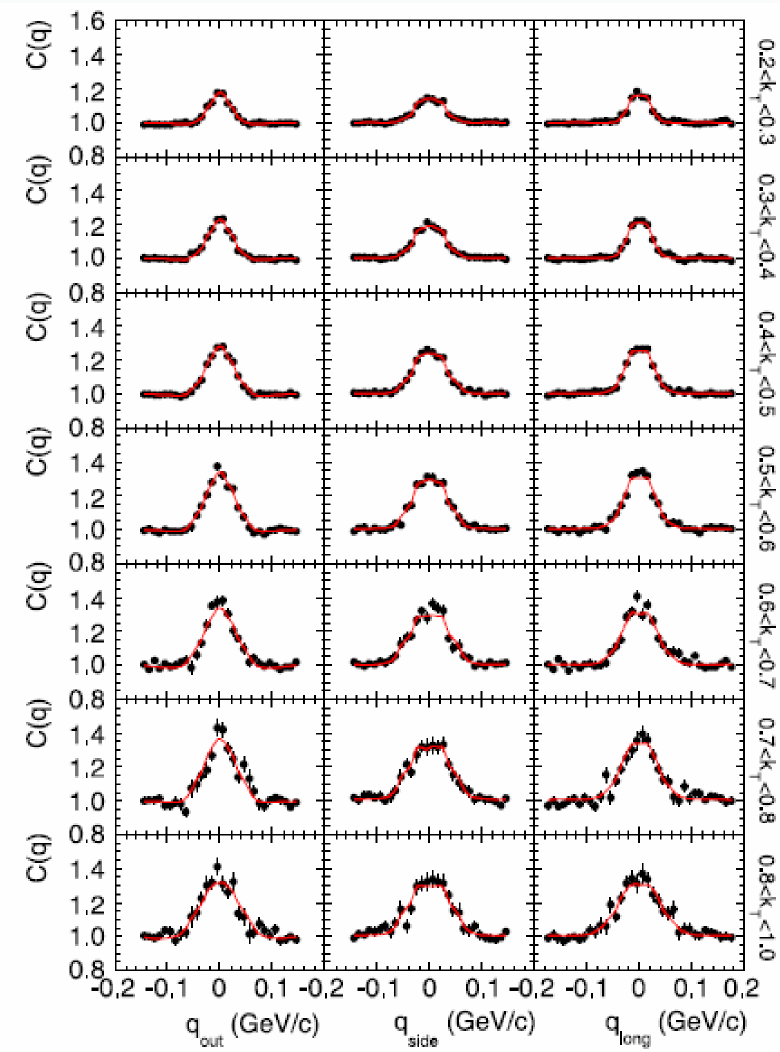

$$C(\mathbf{q}) = \mathcal{N}\left[(1-\lambda) + \lambda K(q_{\text{inv}})\left(1 + G(\mathbf{q})\right)\right],$$
$$G(\mathbf{q}) = \exp\left(-\left(R_{\text{out}}^2 q_{\text{out}}^2 + R_{\text{side}}^2 q_{\text{side}}^2 + R_{\text{long}}^2 q_{\text{long}}^2 + 2|R_{\text{ol}}|R_{\text{ol}} q_{\text{out}} q_{\text{long}}\right)\right),$$

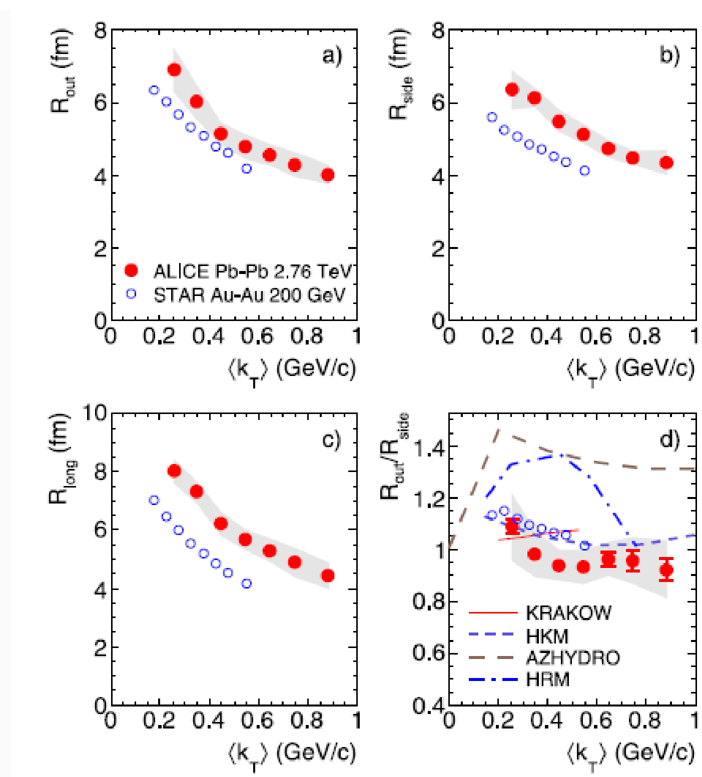

Decreasing trend with increasing k_T.
HBT radii for the 5% most central Pb–Pb collisions at $\sqrt{s_{NN}}$ = 2.76 TeV significantly (10–35%) larger at $\sqrt{s_{NN}}$ = 200 GeV.

Beam energy dependence of the radii

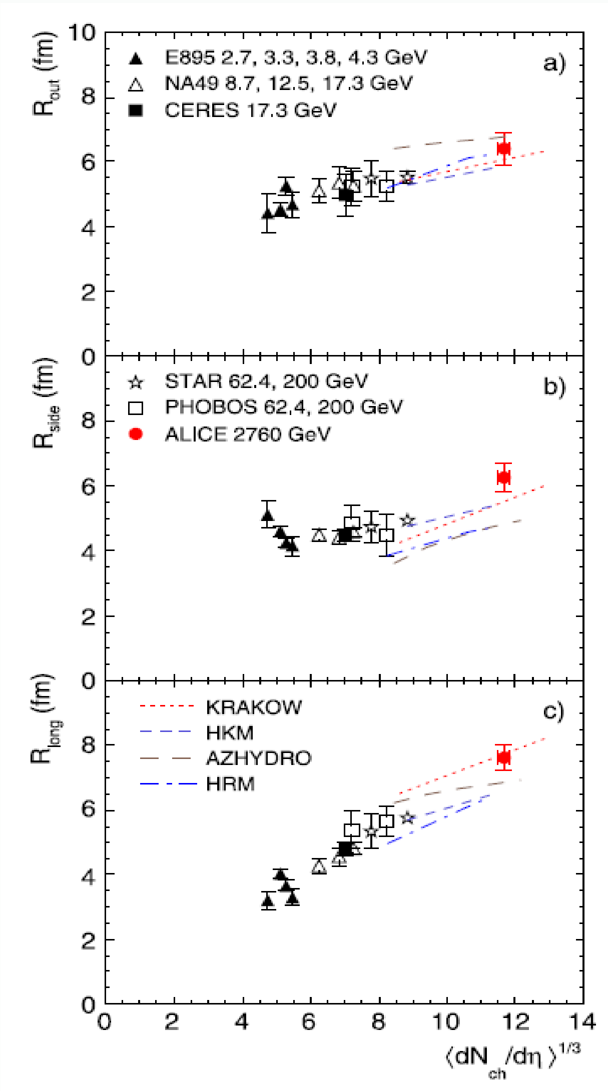

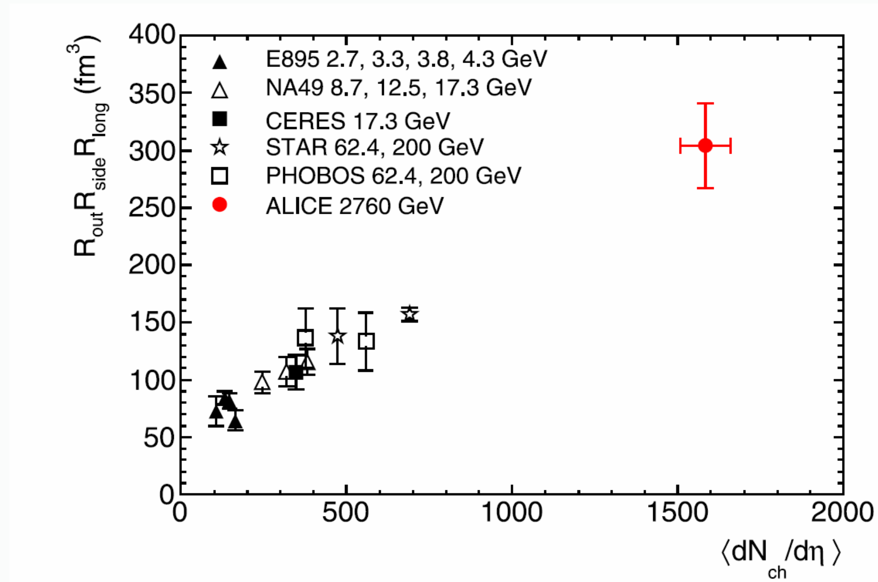

Connected to the volume of the homogeneity region,
Linear dependence on the dN_{ch}/dh
Two times larger at the LHC than at RHIC.

Beam energy dependence of the decoupling time

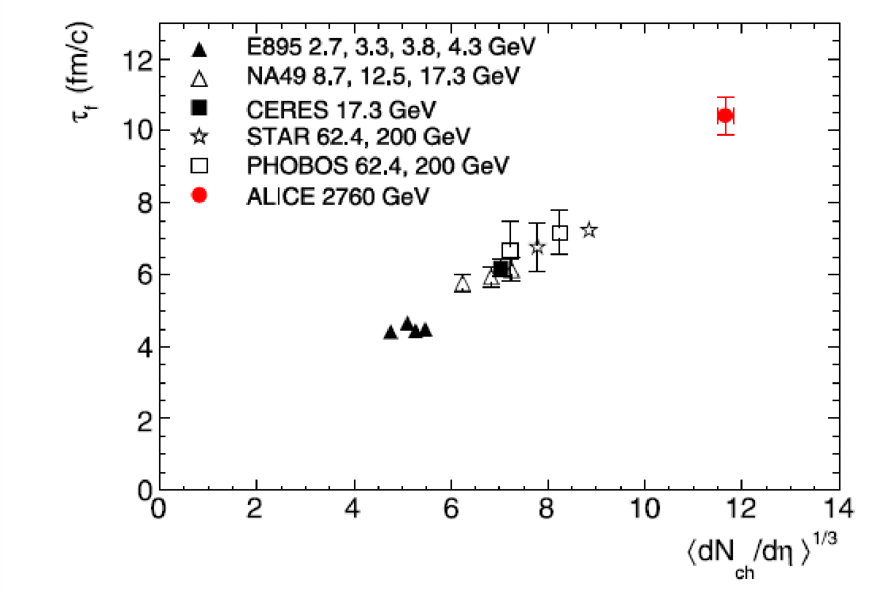

$$R^2_{\text{long}}(k_T) = \frac{\tau_f^2 T}{m_T}\frac{K_2(m_T/T)}{K_1(m_T/T)}, \quad m_T = \sqrt{m_\pi^2 + k_T^2},$$

The decoupling time for midrapidity pions exceeds 10 fm/c which is 40% larger than at RHIC

The fireball formed in nuclear collisions at the LHC is hotter, lives longer, and expands to a larger size at freeze-out as compared to lower energies.

- **backup**

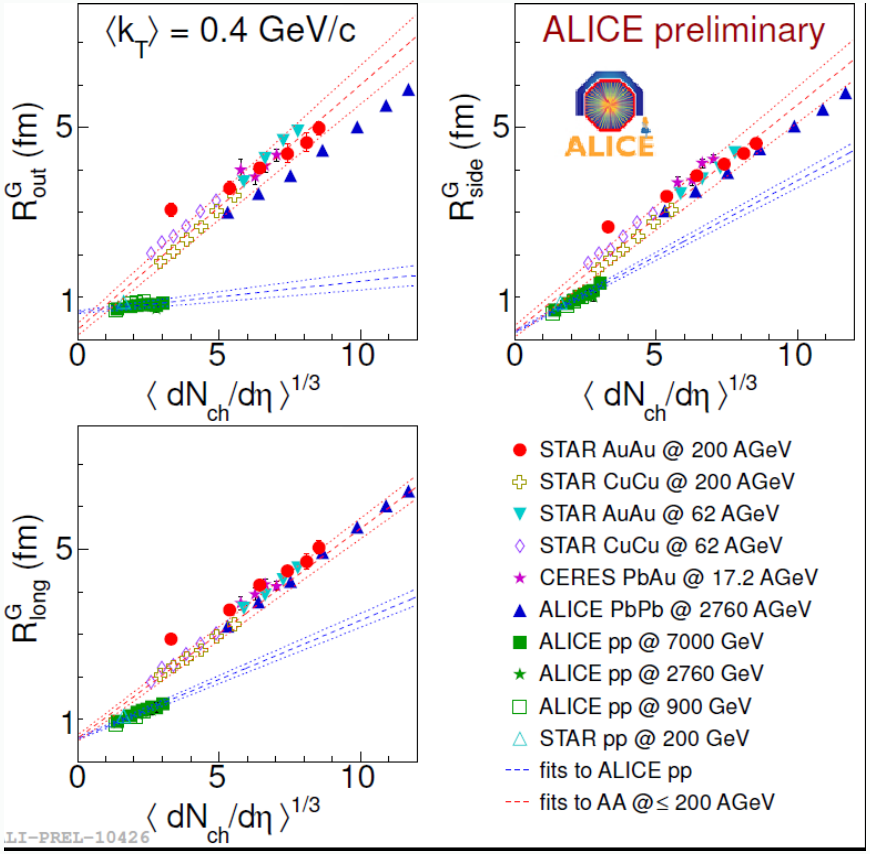

⟨k_T⟩ = 0.4 GeV/c
ALICE preliminary
ALICE
R^G_out (fm)
R^G_side (fm)
R^G_long (fm)
⟨ dN_ch/dη ⟩^1/3
STAR AuAu @ 200 AGeV
STAR CuCu @ 200 AGeV
STAR AuAu @ 62 AGeV
STAR CuCu @ 62 AGeV
CERES PbAu @ 17.2 AGeV
ALICE PbPb @ 2760 AGeV
ALICE pp @ 7000 GeV
ALICE pp @ 2760 GeV
ALICE pp @ 900 GeV
STAR pp @ 200 GeV
fits to ALICE pp
fits to AA @≤ 200 AGeV
LI-PREL-10426

The Time Projection Chamber

Main tracking detector (charged particles) of the ALICE Central Barrel

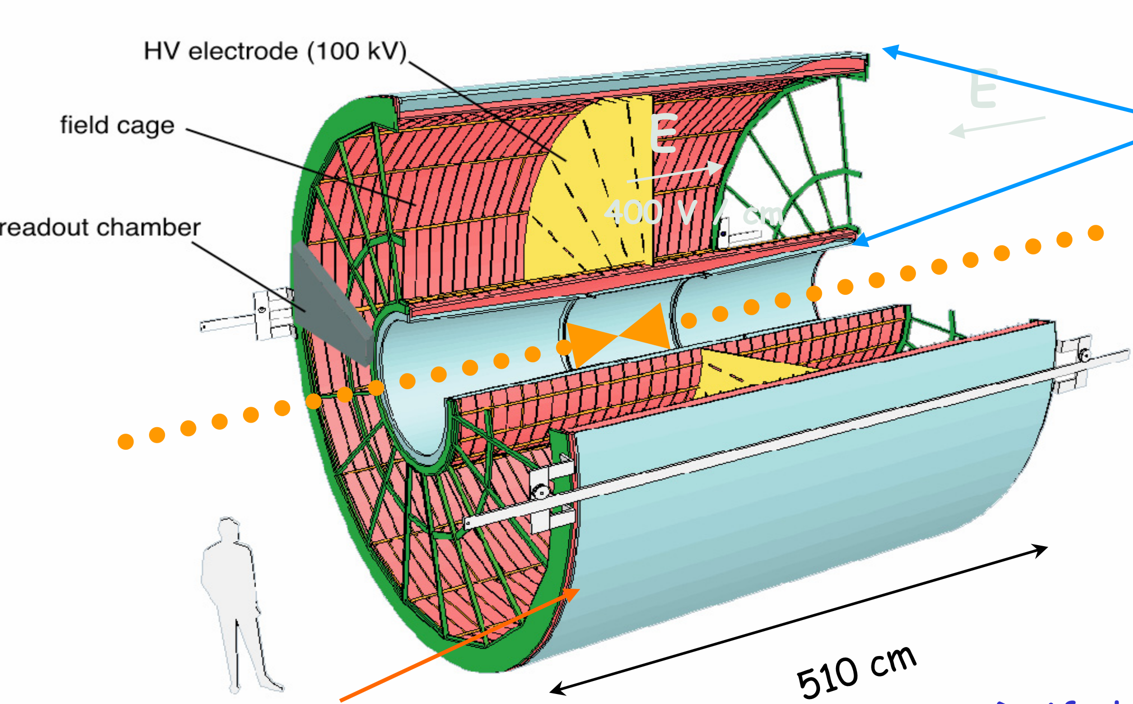

Suspended field defining strips 400 V / cm

Inner and Outer Containment Vessels (150 mm, CO_2)

- very thin & lightweight FC ~3% X_0
- high track density & small space charge
  drift gas, chamber lay-out, field strips, ..

845 < r < 2466 mm
Drift length 2 x 2500 mm
Drift gas $Ne\text{-}CO_2\text{-}N_2$ (86/9/5)
Gas volume 95 m3
557568 readout pads

Functions, Functions, …

$$\frac{dN}{p_T dp_T} \propto \left(1+\frac{p_0}{p_T}\right)^{-n}$$ power law (high-p_T)

$$\frac{dN}{m_T dm_T} \propto m_T \; K_1\left(\frac{m_T}{T}\right) \xrightarrow{m_T>>T} \sqrt{m_T}\, e^{-m_T/T}$$ thermal emission (4π)

$$\frac{dN}{m_T dm_T} \propto m_T e^{-m_T/T}$$ thermal emission (y=0)

$$\frac{dN}{m_T dm_T} \propto \int_0^R r\, dr\, m_T\; I_0\left(\frac{p_T \sinh\rho}{T}\right) K_1\left(\frac{m_T \cosh\rho}{T}\right)$$ thermal + flow

$$\frac{dN}{m_T dm_T} \propto e^{-m_T/T}$$ simple

$$\frac{dN}{m_T dm_T} \propto \frac{e^{-m_T/T}}{m_T{}^{\lambda}}$$ Empirical parametrization from pp (m_T-scaling)

but also from theoretical model (flux-tube + Schwinger)
(Gatoff, Wong, PRD 46, 997 (1992)

Note: "T" depends on function used
in papers often more than one fit function quoted …

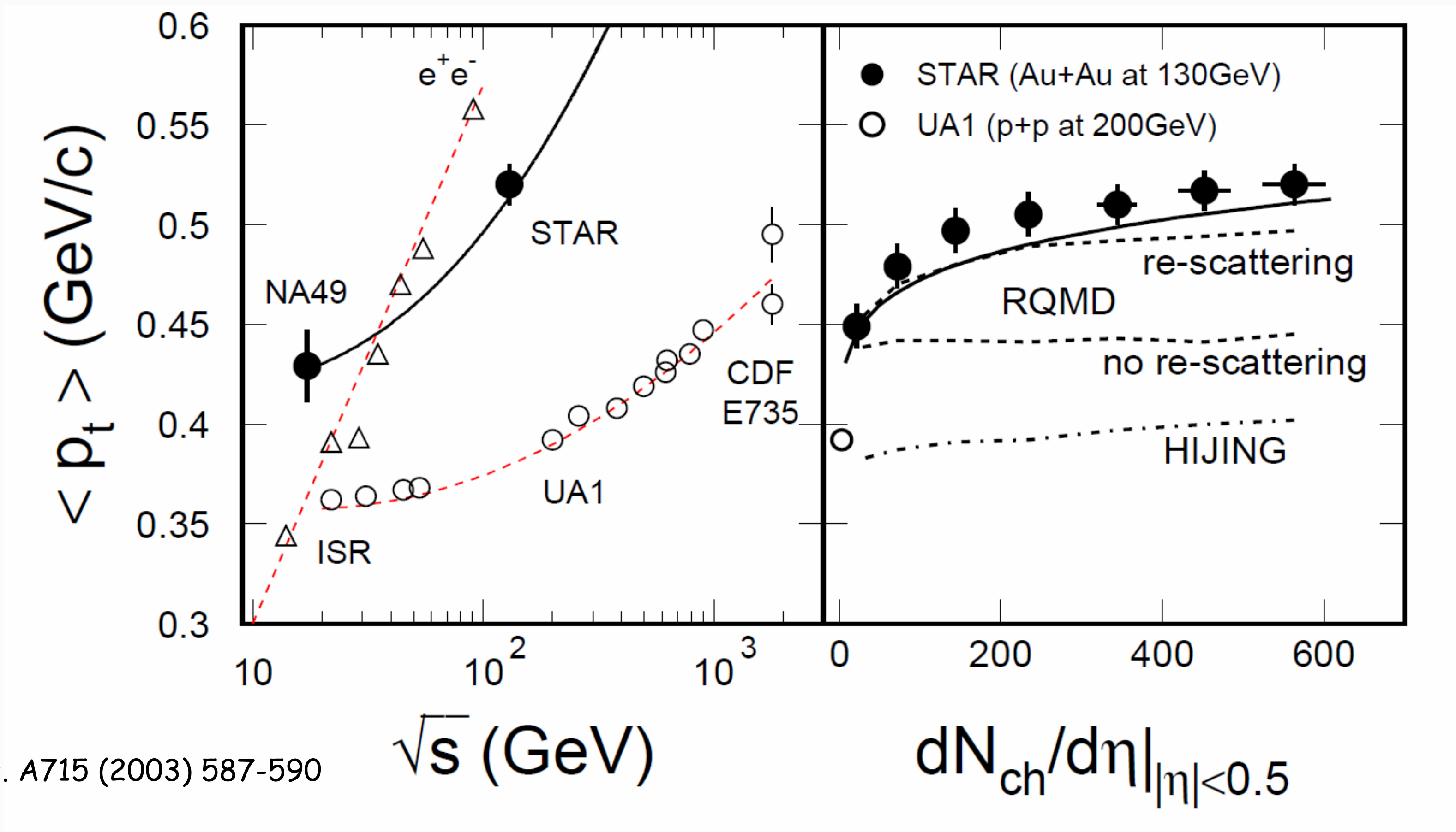

Nucl. Phys. A715 (2003) 587-590

The fact that the $\langle p_t \rangle$ from AA collisions is distinctly different from both pp and e^+e^- indicates that the AA collisions are not simple superpositions of the elementary collisions.